

Explaining anomalies of B -physics, muon $g - 2$ and W mass in R -parity violating MSSM with seesaw mechanism

Min-Di Zheng^{a*}, Feng-Zhi Chen^{a,b†}, and Hong-Hao Zhang^{a‡}

^a School of Physics, Sun Yat-Sen University, Guangzhou 510275, China

^b Key Laboratory of Quark and Lepton Physics (MOE),
Central China Normal University, Wuhan 430079, China

Abstract

The recent experimental results including the $R_{K^{(*)}}$, $R_{D^{(*)}}$, $(g - 2)_\mu$ and W mass show the deviations from the standard model (SM) predictions, implying the clues of the new physics (NP). In this work, we investigate the explanations of these anomalies in the R -parity violating minimal supersymmetric standard model (RPV-MSSM) extended with the inverse seesaw mechanism. The non-unitarity extent η_{ee} and the loop corrections involving the $\lambda' \hat{L} \hat{Q} \hat{D}$ interaction are utilized to raise the m_W prediction through muon decays. We also find that the $\lambda' \hat{L} \hat{Q} \hat{D}$ interaction including the right-handed (RH)/singlet (s)neutrinos can explain the $R_{K^{(*)}}$ and $R_{D^{(*)}}$ anomalies simultaneously when considering nonzero λ'_{1jk} . For nonzero λ'_{2jk} , this model fulfils the whole $b \rightarrow s \ell^+ \ell^-$ fit but cannot be accordant with $R_{D^{(*)}}$ measurements. Furthermore, the explanations in both cases are favored by the $(g - 2)_\mu$ data, neutrino oscillation data and the relevant constraints we scrutinised.

*zhengmd5@mail.sysu.edu.cn

†chenfzh25@mail.sysu.edu.cn

‡zhh98@mail.sysu.edu.cn

1 Introduction

Recently, the experimental measurements implying the lepton flavor universality violation (LFUV) within the semileptonic decays of B -meson, show the striking results. The measurement of the observable, $R_K = \mathcal{B}(B \rightarrow K\mu^+\mu^-)/\mathcal{B}(B \rightarrow Ke^+e^-)$, reported by the LHCb collaboration [1] with the value $R_K = 0.846^{+0.042}_{-0.039} {}^{+0.013}_{-0.012}$ in the q^2 bin $[1.1, 6]$ GeV^2 , deviates from the SM prediction by 3.1σ . The relevant R_{K^*} measurements show the deviations larger than 2σ [2] from the SM. Besides, some discrepancies larger than 2σ , are also reported in several measurements of $b \rightarrow s\mu^+\mu^-$ processes, including the P'_5 [3], the branching ratios $\mathcal{B}(B_s \rightarrow \phi\mu^+\mu^-)$ [4], $\mathcal{B}(B_s \rightarrow \mu^+\mu^-)$ [5–7], etc. As for the charged-current decays of B -meson, the combined result of the experimental observables $R_{D^{(*)}} = \mathcal{B}(B \rightarrow D^{(*)}\tau\nu)/\mathcal{B}(B \rightarrow D^{(*)}\ell\nu)$, given by the Heavy Flavor Averaging Group (HFLAV), is 3.3σ away from the SM prediction, with the relative correlation -0.38 [8]. Thus, the $b \rightarrow s\ell^+\ell^-$ ($\ell = e, \mu$) anomalies, especially the striking R_K deviation, along with the $R_{D^{(*)}}$ deviation, all imply the LFUV anomalies in B -physics.

Apart from the B -physics anomalies, the clues of NP can also be probed in the precision measurements. The latest result of the muon anomalous magnetic moment $a_\mu = (g - 2)_\mu$ in the E989 experiment, is reported by the Fermilab National Accelerator Laboratory (FNAL) that $a_\mu^{\text{FNAL}} = 116592040(54) \times 10^{-11}$ [9], which agrees with the previous result from the E821 experiment at Brookhaven National Laboratory (BNL), $a_\mu^{\text{BNL}} = 116592080(63) \times 10^{-11}$ [10], but is 3.3σ away from the SM prediction $a_\mu^{\text{SM}} = 116591810(43) \times 10^{-11}$ [11]. Combining the two experimental results, the significance deviated from the SM then arrives at the level of 4.2σ ¹. Intriguingly and very recently, another anomaly has been revealed in high precision measurement on the W -boson mass by the Collider Detector at Fermilab (CDF) collaboration at Tevatron. The measured value is $m_W^{\text{CDF-II}} = 80.4335 \pm 0.0094$ GeV [21], which shows 7σ deviation from the SM prediction $m_W^{\text{SM}} = 80.357 \pm 0.006$ GeV [22]. This measurement, if confirmed by other experiments in the future, will change profoundly the trend of NP searches.

Combining the astonishing $m_W^{\text{CDF-II}}$ with the B -physics anomalies and $(g - 2)_\mu$ data, particular NP features are competitive for explanations. In this work, we focus on the supersymmetric (SUSY) models extended by the R -parity violation. As one knows, this framework with the $\lambda \hat{L} \hat{Q} \hat{D}$ superpotential term among the RPV terms, can provide explanations for B -physics

¹Recent lattice calculations for the hadronic vacuum polarization [12–14] induce a weaker tension with this combined measurement result, than the preceding review of various SM predictions [11]. However, these lattice results show a tension with the $e^+e^- \rightarrow \text{hadrons}$ data [12–15]. Readers can see Refs. [16–20] for relevant discussions.

anomalies in the $b \rightarrow s\ell^+\ell^-$ or/and the $b \rightarrow c\tau\nu$ process (see e.g. Refs. [23–26]). In Ref. [27], two of us provide RPV-MSSM extended by the inverse seesaw mechanism (named as RPV-MSSMIS) firstly to explain the $b \rightarrow s\ell^+\ell^-$ anomalies through the RPV-interactions including RH/singlet (s)neutrinos and explain the $(g-2)_\mu$ data through the chirality-flipping. The explanation also fulfils the recent neutrino-oscillation data. Here we ask this question: can this model further accommodate the $R_{D^{(*)}}$ measurements and $m_W^{\text{CDF-II}}$ shift? The simultaneous explanations of the $R_{K^{(*)}}$ and $R_{D^{(*)}}$ anomalies in RPV-MSSM have been studied recently in Refs. [25, 26, 28, 29], while with the experiment data updated, it is straightforward to consider this topic in RPV-MSSMIS. Besides, there are some distinctive model effects on some observables, e.g. the branching fractions of neutrino-produced processes, the extraction of the Fermi constant G_μ and the prediction of W mass. In Ref. [30], we show that the loop-corrections to the vertex $W\ell\nu$ from RPV-interactions can raise the m_W prediction. Interestingly, the engaging of RH neutrinos can also achieve this purpose [31, 32], although the two ways are constrained by the relevant experiments, e.g. the purely leptonic decays of Z -boson, pion and kaon. One can see that the two ways are both included in RPV-MSSMIS, so it is promising to explain (some of) B -physics anomalies, $(g-2)_\mu$ data and m_W shift simultaneously.

Our paper is organized as follows. The model and the theoretical calculations are in section 2. Then we scrutinise the relevant constraints in section 3, which is followed by the numerical results and discussions in section 4. The conclusions are finally made in section 5.

2 The anomaly explanations in RPV-MSSMIS

In this section, we begin to investigate the NP effects on the flavor anomalies, i.e. $b \rightarrow s\ell^+\ell^-$ anomalies, $R_{D^{(*)}}$ deviations and the $(g-2)_\mu$ problem, as well as the new measurement of $m_W^{\text{CDF-II}}$, in the framework of RPV-MSSMIS.

2.1 RPV-MSSMIS framework

First we make some introductions to RPV-MSSMIS [27]. The superpotential and the soft SUSY breaking Lagrangian are respectively given by

$$\begin{aligned}\mathcal{W} = & \mathcal{W}_{\text{MSSM}} + Y_\nu^{ij} \hat{R}_i \hat{L}_j \hat{H}_u + M_R^{ij} \hat{R}_i \hat{S}_j + \frac{1}{2} \mu_S^{ij} \hat{S}_i \hat{S}_j + \lambda'_{ijk} \hat{L}_i \hat{Q}_j \hat{D}_k, \\ -\mathcal{L}^{\text{soft}} = & -\mathcal{L}_{\text{MSSM}}^{\text{soft}} + (m_{\tilde{R}}^2)_{ij} \tilde{R}_i^* \tilde{R}_j + (m_{\tilde{S}}^2)_{ij} \tilde{S}_i^* \tilde{S}_j\end{aligned}$$

$$+ (A_\nu Y_\nu)_{ij} \tilde{R}_i^* \tilde{L}_j H_u + B_{M_R}^{ij} \tilde{R}_i^* \tilde{S}_j + \frac{1}{2} B_{\mu_S}^{ij} \tilde{S}_i \tilde{S}_j, \quad (2.1)$$

where the MSSM parts, $\mathcal{W}_{\text{MSSM}}$ and $\mathcal{L}_{\text{MSSM}}^{\text{soft}}$, can be referred to Refs [33, 34], and the generation indices $i, j, k = 1, 2, 3$ while the colour ones are omitted, and squarks/sleptons are denoted by “ \sim ”. The neutral scalar fields of the two Higgs doublet superfields, $\hat{H}_u = (\hat{H}_u^+, \hat{H}_u^0)^T$ and $\hat{H}_d = (\hat{H}_d^0, \hat{H}_d^-)^T$, acquire the non-zero vacuum expectation value, i.e. $\langle H_u^0 \rangle = v_u$ and $\langle H_d^0 \rangle = v_d$, respectively, and their mixing is expressed by $\tan \beta = v_u/v_d$.

The additional neutrino sector in the superpotential \mathcal{W} provides the neutrino mass spectrum at the tree level, and the 9×9 mass matrix in the basis (ν, R, S) is

$$\mathcal{M}_\nu = \begin{pmatrix} 0 & m_D^T & 0 \\ m_D & 0 & M_R \\ 0 & M_R^T & \mu_S \end{pmatrix}, \quad (2.2)$$

where the Dirac mass matrix $m_D = \frac{1}{\sqrt{2}} v_u Y_\nu^T$. Then \mathcal{M}_ν can be diagonalized through $\mathcal{M}_\nu^{\text{diag}} = \mathcal{V} \mathcal{M}_\nu \mathcal{V}^T$. As to the sneutrino mass square matrix in the basis $(\tilde{\nu}_L^{\mathcal{I}(\mathcal{R})}, \tilde{R}^{\mathcal{I}(\mathcal{R})}, \tilde{S}^{\mathcal{I}(\mathcal{R})})$, it is expressed as

$$\begin{aligned} \mathcal{M}_{\tilde{\nu}^{\mathcal{I}(\mathcal{R})}}^2 &= \begin{pmatrix} m_{\tilde{L}'}^2 & (A_\nu - \mu \cot \beta) m_D^T & m_D^T M_R \\ (A_\nu - \mu \cot \beta) m_D & m_{\tilde{R}}^2 + M_R M_R^T + m_D m_D^T & \pm M_R \mu_S + B_{M_R} \\ M_R^T m_D & \pm \mu_S M_R^T + B_{M_R}^T & m_S^2 + \mu_S^2 + M_R^T M_R \pm B_{\mu_S} \end{pmatrix} \\ &\approx \begin{pmatrix} m_{\tilde{L}'}^2 & (A_\nu - \mu \cot \beta) m_D^T & m_D^T M_R \\ (A_\nu - \mu \cot \beta) m_D & m_{\tilde{R}}^2 + M_R M_R^T + m_D m_D^T & B_{M_R} \\ M_R^T m_D & B_{M_R}^T & M_R^T M_R \end{pmatrix}, \end{aligned} \quad (2.3)$$

where the “ \pm ”, as well as “ $\mathcal{R}(\mathcal{I})$ ”, denotes the CP-even (odd), and the mass square $m_{\tilde{L}'}^2 = m_{\tilde{L}}^2 + \frac{1}{2} m_Z^2 \cos 2\beta + m_D m_D^T$ is regarded as a whole input, with $m_{\tilde{L}}^2$ being the soft mass square of \tilde{L} . Given the value of μ_S is tiny and B_{μ_S} is also relatively small [35], we have made an approximation in Eq. (2.3), which induces the CP-even and CP-odd masses nearly the same. With this approximation, the mixing matrices $\tilde{\mathcal{V}}^{\mathcal{I}(\mathcal{R})}$, which diagonalize sneutrino mass square matrices through $\tilde{\mathcal{V}}^{\mathcal{I}(\mathcal{R})} \mathcal{M}_{\tilde{\nu}^{\mathcal{I}(\mathcal{R})}}^2 \tilde{\mathcal{V}}^{\mathcal{I}(\mathcal{R})\dagger} = (\mathcal{M}_{\tilde{\nu}^{\mathcal{I}(\mathcal{R})}}^2)^{\text{diag}}$, can also be regarded as the same whether CP even or odd. In the rest of the paper, we can replace the $\tilde{\mathcal{V}}^{\mathcal{R}}$ and the physical mass $m_{\tilde{\nu}^{\mathcal{R}}}$ with the corresponding $\tilde{\mathcal{V}}^{\mathcal{I}}$ and $m_{\tilde{\nu}^{\mathcal{I}}}$.

Afterwards we introduce the trilinear RPV interaction in this model. With the superpotential term $\lambda'_{ijk} \hat{L}_i \hat{Q}_j \hat{D}_k$, the relevant Lagrangian in the context of mass eigenstates for the down-type quarks and charged leptons is given by

$$\begin{aligned} \mathcal{L}_{\text{LQD}} = & \lambda'_{vjk} \tilde{\nu}_v \bar{d}_{Rk} d_{Lj} + \lambda'_{vjk} (\tilde{d}_{Lj} \bar{d}_{Rk} \nu_v + \tilde{d}_{Rk}^* \bar{\nu}_v^c d_{Lj}) \\ & - \tilde{\lambda}'_{ilk} (\tilde{l}_{Li} \bar{d}_{Rk} u_{Ll} + \tilde{u}_{Ll} \bar{d}_{Rk} l_{Li} + \tilde{d}_{Rk}^* \bar{l}_{Li}^c u_{Ll}) + \text{h.c.}, \end{aligned} \quad (2.4)$$

where “ c ” indicates the charge conjugated fermions, and the fields $\tilde{\nu}_L$, ν_L and u_L (aligned with \tilde{u}_L) in the flavor basis have been rotated into mass eigenstates by the mixing matrices $\tilde{\mathcal{V}}^{\mathcal{I}}$, \mathcal{V} and K , respectively. Concretely, the indices $v = 1, 2, \dots, 9$ denote the generation of the physical (s)neutrinos, and the three λ' couplings are deduced as $\lambda'_{vjk} = \lambda'_{ijk} \tilde{\mathcal{V}}_{vi}^{\mathcal{I}*}$, $\lambda'_{vjk} = \lambda'_{ijk} \mathcal{V}_{vi}$ and $\tilde{\lambda}'_{ilk} = \lambda'_{ijk} K_{lj}^*$. In the following, the interaction (diagram) involving these λ' couplings is called the λ' interaction (diagram).

By the end of this section, we mention the chargino matrix from the MSSM sector, which is [34]

$$\mathcal{M}_{\chi^\pm} = \begin{pmatrix} M_2 & \frac{ev_u}{\sqrt{2} \sin \theta_W} \\ \frac{ev_d}{\sqrt{2} \sin \theta_W} & \mu \end{pmatrix}, \quad (2.5)$$

where M_2 being the wino mass and μ being the Higgsino mass in the flavor basis, and θ_W is the Weinberg angle. The mixing matrix V and U diagonalize \mathcal{M}_{χ^\pm} by $U^* \mathcal{M}_{\chi^\pm} V^\dagger = \mathcal{M}_{\chi^\pm}^{\text{diag}}$. For a review on the neutralino matrix, readers are also referred to Ref. [34].

2.2 $b \rightarrow s \ell^+ \ell^-$ anomalies

To study the NP effects on the $b \rightarrow s \ell^+ \ell^-$ process, the relevant Lagrangian of the low energy effective field theory is

$$\mathcal{L}_{\text{eff}}^{bs\ell\ell} = \frac{4G_F}{\sqrt{2}} \eta_t \sum_i C_i \mathcal{O}_i + \text{h.c.}, \quad (2.6)$$

where the CKM factor $\eta_t \equiv K_{tb} K_{ts}^*$. The most favored operators to explain the $b \rightarrow s \ell^+ \ell^-$ anomalies are

$$\mathcal{O}_9 = \frac{e^2}{16\pi^2} (\bar{s} \gamma_\mu P_L b) (\bar{\ell} \gamma^\mu \ell), \quad \mathcal{O}_{10} = \frac{e^2}{16\pi^2} (\bar{s} \gamma_\mu P_L b) (\bar{\ell} \gamma^\mu \gamma_5 \ell), \quad (2.7)$$

where $P_L = (1 - \gamma_5)/2$ is the left-handed (LH) chirality projector, and the Wilson coefficients $C_{9(10)} = C_{9(10)}^{\text{SM}} + C_{9(10)}^{\text{NP}}$. Then with the results of the model-independent global fit [36–50], the RPV-MSSMIS can provide NP contributions which dominate the $\mu\mu(ee)$ channel, i.e. $\Delta C_{9\mu} = -\Delta C_{10\mu} < 0$ or $\Delta C_{9e} = -\Delta C_{10e} > 0$, to explain the $R_{K^{(*)}}$ anomaly. Especially, the case $\Delta C_{9\mu} = -\Delta C_{10\mu} < 0$ can be further in accord with the deviations of $b \rightarrow s\mu^+\mu^-$ measurements from the SM predictions, e.g. measurements of $B_s \rightarrow \mu^+\mu^-$ [5–7] and $B_s \rightarrow \phi\mu^+\mu^-$ [4, 51].

In RPV-MSSMIS, we set sleptons and winos with masses of several 10^2 GeV while the masses of all colored sparticles are around TeV or above, and all the model parameters are set at the scale $\mu_{\text{NP}} = 0.5$ TeV. To eliminate the unfavored contributions to $C_{9(10)}^{\text{NP}}$ (the operator $\mathcal{O}'_{9(10)}$ is given by replacing P_L with P_R in $\mathcal{O}_{9(10)}$), we assume the coupling λ'_{ijk} is non-negligible only for the single value k at μ_{NP} scale [27]. Then the dominant contributions to $\Delta C_{9\ell} = -\Delta C_{10\ell}$ in RPV-MSSMIS are given by

$$\Delta C_{9\ell}^{\tilde{\nu}-\chi^\pm} = \lambda_{v3k}^{\mathcal{I}} \lambda_{v'2k}^{\mathcal{I}*} (g_2 V_{m1}^* \tilde{\mathcal{V}}_{v\ell}^{\mathcal{I}} - V_{m2}^* Y_{\ell v}^{\mathcal{I}}) (g_2 V_{m1} \tilde{\mathcal{V}}_{v'\ell}^{\mathcal{I}} - V_{m2} Y_{\ell v'}^{\mathcal{I}}) D_2[m_{\tilde{\nu}_v^{\mathcal{I}}}, m_{\tilde{\nu}_{v'}^{\mathcal{I}}}, m_{\chi_m^\pm}, m_b], \quad (2.8)$$

where the formula of Passarino-Veltman function [52] D_2 is collected in appendix A, and the coupling $Y_{\ell v}^{\mathcal{I}} \equiv (Y_\nu)_{j\ell} \tilde{\mathcal{V}}_{v(j+3)}^{\mathcal{I}*}$. One can see that the light sneutrinos and winos will help provide considerable LFUV effects. The Wilson coefficient of Eq. (2.8) is proportional to the product $\lambda'_{2(1)3k} \lambda_{2(1)2k}^*$, which is related to the $\mu\mu(ee)$ -channel contribution, assuming that no flavor transitions within sneutrino sectors. In the appendix A, we provide the whole list of formulas from the scrutinized one-loop box diagrams of the $b \rightarrow s\ell^+\ell^-$ process, which are adopted in the numerical calculations. Under the assumption of single value k , only the LH-quark-vector-current contributions $\Delta C_{9(10)\ell}^{\text{NP}}(\mu_{\text{NP}})$ exist, and the RH-quark-vector-current contributions $\Delta C_{9(10)\ell}^{\text{NP}}(\mu_{\text{NP}})$ vanish. Due to the approximate conservation of (axial-)vector currents, $\Delta C_{9(10)\ell}^{\text{NP}}(\mu_b) = \Delta C_{9(10)\ell}^{\text{NP}}(\mu_{\text{NP}})$ and $\Delta C_{9(10)\ell}^{\text{NP}}(\mu_b)$ still vanish when run down to the scale $\mu_b = m_b$ through QCD renormalization. Then we can adopt the results at μ_b from the model-independent global fit in Ref. [42], to constrain the model inputs. The fit results show $\Delta C_{9e} = -\Delta C_{10e} = 0.37 \pm 0.10$ as the best fit for the $R_{K^{(*)}}$ explanations in the ee channel. As for the $\mu\mu$ channel, $\Delta C_{9\mu} = -\Delta C_{10\mu} = -0.35 \pm 0.08$ and $\Delta C_{9\mu} = -\Delta C_{10\mu} = -0.39 \pm 0.07$ are utilized to explain $R_{K^{(*)}}$ and the whole $b \rightarrow s\ell^+\ell^-$ anomaly, respectively. In this work, we restrict $k = 3$ for a benchmark, and consider one of $(\lambda'_{1j3}, \lambda'_{2j3})$ nonzero at a time, i.e. $\lambda'_{2(1)j3} = 0$ at μ_{NP} scale for Case A(B).

2.3 $R_{D^{(*)}}$ anomalies

Next we turn to the $R_{D^{(*)}}$, implying the LFUV anomalies in the charged current $b \rightarrow c\tau\nu$. For the generic charged current process $d_j \rightarrow u_n l_l \nu$, the effective Lagrangian is

$$\mathcal{L}_{\text{eff}}^{dul\nu} = -\frac{4G_F}{\sqrt{2}} K_{nj} (\mathcal{V}_{li}^T + C_{njli}) \bar{u}_n \gamma_\mu P_L d_j \bar{l}_l \gamma^\mu P_L \nu_i + \text{h.c.}, \quad (2.9)$$

where the first term in the bracket gives the SM contribution combined with the neutrino-generation mixing, and the second term is related to the λ' interactions, with the formula

$$C_{njli} = \frac{\mathcal{V}_{\alpha i}^T \lambda'_{\alpha j 3} \tilde{\lambda}_{ln3}^*}{4\sqrt{2}G_F K_{nj} m_{b_R}^2} \equiv \mathcal{V}_{\alpha i}^T \lambda'_{\alpha j 3} C'_{njl}. \quad (2.10)$$

It is useful to define the ratio

$$\begin{aligned} R_{njl} &\equiv \frac{\mathcal{B}(d_j \rightarrow u_n l_l \nu)_{\text{SM+NP}}}{\mathcal{B}(d_j \rightarrow u_n l_l \nu)_{\text{SM}}} = \frac{\sum_{i=1}^3 |K_{nj}|^2 |\mathcal{V}_{li}^T + C_{njli}|^2}{\sum_{i=1}^3 |K_{nj} \delta_{li}|^2} \\ &= \sum_{i=1}^3 |\mathcal{V}_{i' i}^T|^2 |\delta_{li'} + \lambda'_{i' j 3} C'_{njl}|^2, \end{aligned} \quad (2.11)$$

which approximates the ratio in ordinary RPV-MSSM (see Eq. (24) in Ref. [28]) under the nearly unitarity bound of $\mathcal{V}_{3 \times 3}^T$. Then we get,

$$\frac{R_D}{R_D^{\text{SM}}} = \frac{R_{D^*}}{R_{D^*}^{\text{SM}}} = \frac{2R_{233}}{R_{232} + R_{231}}, \quad (2.12)$$

which is named as $\mathcal{R}_{D^{(*)}}^{\text{NP/SM}}$ in this work. We utilize the $R_{D^{(*)}}$ world average with the so-called correlation $\rho_{D^{**}}$, which denotes the $B \rightarrow D^{**} \ell \bar{\nu}_\ell$ correlation structure across R_D and R_{D^*} measurements, as 0 [53]. This result is similar to the one of HFLAV [8]. Then in the situation of this model, we get the fit value of the ratio $\mathcal{R}_{D^{(*)}}^{\text{NP/SM}} = 1.140 \pm 0.045$.

2.4 m_W shift

Here we discuss the NP contributions to the W -boson mass, from the $W\ell\nu$ -vertex loop corrections involving λ' couplings and the non-unitarity of $\mathcal{V}_{3 \times 3}^T$ in this model.

The non-unitarity of $\mathcal{V}_{3 \times 3}^T$ can be shown in

$$(\mathcal{V}_{3 \times 3}^T)_{\alpha i} = (\delta_{\alpha\beta} + \eta_{\alpha\beta})\mathcal{U}_{\beta i}, \quad (2.13)$$

where \mathcal{U} is unitary and the Hermitian η describes the non-unitarity extent. In the inverse seesaw framework, one can figure out $\eta \approx -\frac{1}{2}m_D^\dagger(M_R^*)^{-1}(M_R^T)^{-1}m_D$.

Then we turn to the $Wl\nu$ -vertex expressed in the Lagrangian,

$$\mathcal{L}_{\text{eff}}^{Wl\nu} = \frac{e}{\sqrt{2}\sin\theta_W}\bar{l}_l\gamma^\mu P_L(\mathcal{V}_{li}^T + h_{li})\nu_i W_\mu^- + \text{h.c.}, \quad (2.14)$$

where the first part in the bracket shows the SM contribution combined with the neutrino-generation mixing. The \mathcal{V}_{li}^T term here, can be replaced by $\delta_{li} + \eta_{li}$ by dropping out the \mathcal{U} matrix due to the limit of vanishing m_{ν_i} [54]. The one-loop correction part, h_{li} , is dominated by the λ' contribution h'_{li} . As the analogy to the formula [55], this contribution is given by [30]

$$h'_{li} = -\frac{3}{64\pi^2}x_{\tilde{b}_R}f_W(x_{\tilde{b}_R})\tilde{\lambda}_{l33}^*\tilde{\lambda}'_{i33}, \quad (2.15)$$

where $x_{\tilde{b}_R} \equiv m_t^2/m_{\tilde{b}_R}^2$ and the loop function $f_W(x) \equiv \frac{1}{x-1} + \frac{(x-2)\log x}{(x-1)^2}$, and other minor parts including the ones proportional to $\eta h'$ product are eliminated. This dominant part is from the $u_i d_i \tilde{b}_R$ loop diagram, in which the engaging top quark with large mass and couplings $\tilde{\lambda}'_{l(i)33}$ make h'_{li} dominant.

Since h' and η can contribute to the $Wl\nu$ process at the same level, they both affect the muon decay and induce (see similar formulas in Refs. [31, 54])

$$G_\mu = G_F(1 + \eta_{\ell\ell} + h'_{\ell\ell}), \quad (2.16)$$

where G_μ is the Fermi constant extracted from the muon lifetime, while G_F corresponds to the one in the SM. When m_D and M_R are set diagonal, η can be diagonal. Since we consider the index i in the λ'_{ijk} as 1 or 2 at a time, the matrix h' is also diagonal. Then the prediction of m_W is given by

$$\frac{m_W^2}{m_Z^2} = \frac{1}{2} + \sqrt{\frac{1}{4} - \frac{\pi\alpha}{\sqrt{2}G_\mu m_Z^2}(1 + \eta_{\ell\ell} + \Delta r_0 + h'_{\ell\ell})}, \quad (2.17)$$

where Δr_0 represents the loop corrections from SM and pure MSSM. The MSSM contributes

mainly to the W self-energy, that is not considered in this work by setting sufficiently heavy up-type squarks. One can see that the negative values of $h'_{\ell\ell}$ or/and $\eta_{\ell\ell}$ can raise the prediction of m_W to approach to the CDF-II measurement. Besides, these two variants are related to the CKM elements extraction, which can be described as

$$K_{ud}^\beta = K_{ud}(1 - \eta_{\mu\mu} - h'_{\mu\mu}), \quad (2.18)$$

where K_{ud}^β is extracted from beta decays. The η_{ee} and h'_{ee} terms enter both the $We\nu$ vertex and G_μ , which induces the cancelling in Eq. (2.18). With the extraction of K_{ud} and the analogous ones of K_{us} from kaon decays, it is found that the positive values of $\eta_{\mu\mu} + h'_{\mu\mu}$ are needed to alleviate the Cabbibo anomaly showing around 3σ tension, and besides, the simple RH-neutrino extension cannot fully explain the data [56]. Given the inverse seesaw framework provides negative $\eta_{\ell\ell}$, and $h'_{\ell\ell}$ is also negative commonly, we can set model parameters to make both $|\eta_{\mu\mu}|$ and $|h'_{\mu\mu}|$ sufficiently small to avoid this tension getting worse. Thus, in Case A as defined in section 2.2, we need relative large $|\eta_{ee} + h'_{ee}| \gtrsim 2 \times 10^{-3}$ favored to raise the m_W , with $|\eta_{\mu\mu}| \sim 10^{-4}$; while in Case B, there are $|\eta_{ee}| \gtrsim 2 \times 10^{-3}$ with $|\eta_{\mu\mu}|$ and $|h'_{\mu\mu}|$ around 10^{-4} . It is worth mentioning that other measurements of $\sin\theta_W$, which are in tension with the new $m_W^{\text{CDF-II}}$, also constrain η_{ee} [57–59], e.g. $|\eta_{ee}| < 1.3 \times 10^{-3}$ [59]. In this work, this bound is not considered as the essential one.

2.5 $(g - 2)_\mu$

During the end of section 2, we will mention the NP contributions to a_μ in RPV-MSSMIS. Here we utilize the one-loop chargino and neutralino contributions mainly to explain a_μ data, and these contributions to a_ℓ are given by [27],

$$\begin{aligned} \delta a_\ell^{\chi^\pm} &= \frac{m_\ell}{16\pi^2} \left[\frac{m_\ell}{6m_{\tilde{\nu}_v}^2} (|c_{mv}^{\ell L}|^2 + |c_{mv}^{\ell R}|^2) F_1^C(m_{\chi_m^\pm}^2/m_{\tilde{\nu}_v}^2) + \frac{m_{\chi_m^\pm}}{m_{\tilde{\nu}_v}^2} \text{Re}(c_{mv}^{\ell L} c_{mv}^{\ell R}) F_2^C(m_{\chi_m^\pm}^2/m_{\tilde{\nu}_v}^2) \right], \\ \delta a_\ell^{\chi^0} &= \frac{m_\ell}{16\pi^2} \left[-\frac{m_\ell}{6m_{\tilde{l}_i}^2} (|n_{ni}^{\ell L}|^2 + |n_{ni}^{\ell R}|^2) F_1^N(m_{\chi_n^0}^2/m_{\tilde{l}_i}^2) + \frac{m_{\chi_n^0}}{m_{\tilde{l}_i}^2} \text{Re}(n_{ni}^{\ell L} n_{ni}^{\ell R}) F_2^N(m_{\chi_n^0}^2/m_{\tilde{l}_i}^2) \right], \end{aligned} \quad (2.19)$$

where,

$$c_{mv}^{\ell R} = y_\ell U_{m2} \tilde{\mathcal{V}}_{v\ell}^{\mathcal{I}}, \quad c_{mv}^{\ell L} = -g_2 V_{m1} \tilde{\mathcal{V}}_{v\ell}^{\mathcal{I}} + V_{m2} Y_{\ell v}^{\mathcal{I}};$$

$$n_{ni}^{\ell R} = \sqrt{2}g_1 N_{n1} \delta_{i(\ell+3)} + y_\ell N_{n3} \delta_{i\ell}, \quad n_{ni}^{\ell L} = \frac{1}{\sqrt{2}} (g_2 N_{n2} + g_1 N_{n1}) \delta_{i\ell} - y_\ell N_{n3} \delta_{i(\ell+3)}, \quad (2.20)$$

with the factor functions,

$$\begin{aligned} F_1^C(x) &= \frac{1}{(1-x)^4} (2 + 3x - 6x^2 + x^3 + 6x \log x), \\ F_2^C(x) &= -\frac{1}{(1-x)^3} (3 - 4x + x^2 + 2 \log x), \\ F_1^N(x) &= \frac{1}{(1-x)^4} (1 - 6x + 3x^2 + 2x^3 - 6x^2 \log x), \\ F_2^N(x) &= \frac{1}{(1-x)^3} (1 - x^2 + 2x \log x). \end{aligned} \quad (2.21)$$

Also, the contribution from the λ' diagrams, $\delta a_\ell^{\lambda'} = m_\ell^2 |\lambda'_{\ell j 3}|^2 / 32 \pi^2 m_{\tilde{b}_R}^2$ [26], is not dominant here. In comparison with the original MSSM, the extra $V_{m2} Y_{\ell v}^{\mathcal{I}}$ term in the $c_{mv}^{\ell L}$ of Eq. (2.19) contributes to the chirality flip. With the measured deviation $\Delta a_\mu = a_\mu^{\text{exp}} - a_\mu^{\text{SM}} = (2.51 \pm 0.59) \times 10^{-9}$ [9], the explanation favors $1.33 < |\delta a_\mu^{\chi^\pm} + \delta a_\mu^{\chi^0} + \delta a_\mu^{\lambda'}| \times 10^9 < 3.69$ at 2σ level.

3 The constraints

Before the numerical explanations of the anomalies introduced above, the relevant experimental constraints should be scrutinised to determine the setting of parameter inputs.

3.1 Direct searches

First we consider direct searches for NP particles. The no signs of the SUSY particles until the end of the LHC run II which reaching around 140 fb^{-1} at the center energy 13 TeV, induces the stringent bounds on SUSY models. The allowed masses of colored sparticles, such as gluinos, the first-two generation squarks, stops and sbottoms have been excluded up to 1 – 2 TeV scale [60–66]. In this work, the colored sparticles, except RH sbottoms \tilde{b}_R , are all set around 10 TeV, whereas the masses of \tilde{b}_R , sleptons, charginos, neutralinos, charged Higgs and the heavy neutrinos are all around $10^2 - 10^3$ GeV. Some recent experiments have pushed the upper limit of slepton masses over TeV scale [67–69], however, these searches consider nonzero λ , within the superpotential $\lambda_{ijk} \hat{L}_i \hat{L}_j \hat{E}_k$. Given that we only consider nonzero λ' in the model, so processes of purely leptonic decays of sleptons can be neglected, and one can focus on sleptons decaying to the lightest neutralino χ^0 and leptons. Although the dijet resonance pairs can emerge from

pair-produced sleptons through the λ' interactions, this provides relatively weak bounds due to the large QCD background [70]. Thus, we take the compressed scenario, $m_{\chi_1^\pm} \gtrsim m_{\chi_1^0} \gtrsim 300$ GeV as well as $m_{\tilde{t}_L} > 300$ GeV, based on the recent data [71, 72].

3.2 Tree-level processes

As we set RH sbottoms not decoupled, the tree-level processes exchanging sbottoms will make constraints on the model parameters, and these relevant processes include $B \rightarrow K^{(*)}\nu\bar{\nu}$, $B \rightarrow \pi\nu\bar{\nu}$, $K^+ \rightarrow \pi^+\nu\bar{\nu}$, $D^0 \rightarrow \ell^+\ell^-$, $\tau \rightarrow \ell\rho^0$ as well as the charged current processes $B \rightarrow \tau\nu$, $D_s \rightarrow \tau\nu$, $\tau \rightarrow K(\pi)\nu$ and $\pi \rightarrow \ell\nu(\gamma)$. The first to be introduced are the semilepton decays $B \rightarrow K^{(*)}\nu\bar{\nu}$, $B \rightarrow \pi\nu\bar{\nu}$ and $K^+ \rightarrow \pi^+\nu\bar{\nu}$ involving $d_j \rightarrow d_m\nu_i\bar{\nu}_{i'}$, and the related effective Lagrangian is defined by,

$$\mathcal{L}_{\text{eff}}^{dd\nu\bar{\nu}} = (C_{mj}^{\text{SM}}\delta_{ii'} + C_{mj}^{\nu_i\bar{\nu}_{i'}})(\bar{d}_m\gamma_\mu P_L d_j)(\bar{\nu}_i\gamma^\mu P_L \nu_{i'}) + \text{h.c.}, \quad (3.1)$$

where the SM contribution is $C_{mj}^{\text{SM}} = -\frac{\sqrt{2}G_F e^2 K_{tj} K_{tm}^*}{4\pi^2 \sin^2 \theta_W} X(x_t)$ and the loop function $X(x_t) \equiv \frac{x_t(x_t+2)}{8(x_t-1)} + \frac{3x_t(x_t-2)}{8(x_t-1)^2} \log(x_t)$ with $x_t \equiv m_t^2/m_W^2$ [73]. The NP contributions are

$$C_{mj}^{\nu_i\bar{\nu}_{i'}} = \frac{\lambda_{i'j3}^{\mathcal{N}} \lambda_{im3}^{\mathcal{N}*}}{2m_{b_R}^2} = \frac{\mathcal{V}_{i'\alpha'} \mathcal{V}_{i\alpha}^* \lambda_{\alpha'j3}^{\mathcal{N}} \lambda_{\alpha m3}^{\mathcal{N}*}}{2m_{b_R}^2}. \quad (3.2)$$

It is worth mentioning that the difference between Eq. (3.2) and the corresponding formula in the ordinary RPV-MSSM [74] is the neutrino-generation mixing in λ' interactions. With Eq. (2.13), we can further get

$$C_{mj}^{\nu_i\bar{\nu}_{i'}} \approx \frac{\mathcal{U}_{\alpha'i'} \mathcal{U}_{\alpha i}^* \lambda_{\alpha'j3}^{\mathcal{N}} \lambda_{\alpha m3}^{\mathcal{N}*}}{2m_{b_R}^2}. \quad (3.3)$$

Given \mathcal{U} is not a diagonal-like matrix, the NP effects on this process are unique compared to RPV-MSSM.

The experimental measurement $\mathcal{B}(K^+ \rightarrow \pi^+\nu\bar{\nu})_{\text{exp}} = (1.7 \pm 1.1) \times 10^{-10}$ [75] combined with the SM prediction $\mathcal{B}(K^+ \rightarrow \pi^+\nu\bar{\nu})_{\text{SM}} = (9.24 \pm 0.83) \times 10^{-11}$ [76] induces the strong constraint that $|\lambda_{i'2k}^{\mathcal{N}} \lambda_{i1k}^{\mathcal{N}*}| < 7.4 \times 10^{-4} (m_{b_R}/1\text{TeV})^2$ [28], thus, we assume $\lambda_{i1k}^{\mathcal{N}}$ negligible to avoid the bound and then the $B \rightarrow \pi\nu\bar{\nu}$ process will also make no bound.

Then we investigate the constraint from $B \rightarrow K^{(*)}\nu\bar{\nu}$. One can define the ratio,

$$R_{K^{(*)}}^{\nu\bar{\nu}} \equiv \frac{\mathcal{B}(b \rightarrow s\nu\bar{\nu})_{\text{NP+SM}}}{\mathcal{B}(b \rightarrow s\nu\bar{\nu})_{\text{SM}}} = \frac{\sum_{i=1}^3 |C_{23}^{\text{SM}} + C_{23}^{\nu_i\bar{\nu}_i}|^2 + \sum_{i \neq i'}^3 |C_{23}^{\nu_i\bar{\nu}_{i'}}|^2}{3|C_{23}^{\text{SM}}|^2}. \quad (3.4)$$

The related experimental data [77, 78] and SM predictions [73, 79] provide $R_K^{\nu\bar{\nu}} = 2.4 \pm 0.9$ for $B \rightarrow K^+\nu\bar{\nu}$ and the upper limit $R_{K^*}^{\nu\bar{\nu}} < 2.7$ at 90% confidence level (CL) for $B \rightarrow K^*\nu\bar{\nu}$.

We collect the experimental results and SM predictions of $D^0 \rightarrow \ell^+\ell^-$, $\tau \rightarrow \ell\rho^0$ decays with the charged current processes, $B \rightarrow \tau\nu$, $D_s \rightarrow \tau\nu$ and $\tau \rightarrow K\nu$, as well as the processes discussed above in table 1. Following the same/analogical numerical calculations in the ordinary RPV-MSSM (see Refs. [28, 80]), the constraint from $\mathcal{B}(D^0 \rightarrow \mu^+\mu^-)$ gives $|\lambda'_{223}|^2 < 0.31(m_{\tilde{b}_R}/1\text{TeV})^2$, while the one from $\mathcal{B}(D^0 \rightarrow e^+e^-)$ is negligible due to the small m_e , and the bound from $\mathcal{B}(\tau \rightarrow \mu(e)\rho^0)$ provides $|\lambda'_{323}\lambda_{2(1)23}^*| < 0.38(m_{\tilde{b}_R}/1\text{TeV})^2$. Besides, the R_{133} , R_{223} and R_{123} , expressing the ratios of the measurement values to the SM predictions for $\mathcal{B}(B \rightarrow \tau\nu)$, $\mathcal{B}(D_s \rightarrow \tau\nu)$ and $\mathcal{B}(\tau \rightarrow K\nu)$ respectively, are also constrained. As for the $\pi \rightarrow \ell\nu(\gamma)$ decay, similar to the formula in Ref. [54], the bound (including loop corrections h') is given by

$$\frac{1 + \eta_{\mu\mu} + h'_{\mu\mu}}{1 + \eta_{ee} + h'_{ee}} = 1.0010(9), \quad (3.5)$$

which can be translated into $|\eta_{ee} + h'_{ee}| \lesssim 0.0028$ within the 2σ level, for negligible $\eta(h')_{\mu\mu}$. The \mathcal{V} matrix is also bounded by the $\tau(\mu)$ decaying to charged leptons and neutrinos at the tree level, while both \mathcal{V} and λ' couplings are constrained by these decays as well as the charged lepton flavor violating (cLFV) decays at one-loop level, which will be addressed in section 3.3.

3.3 Loop-level processes

Here we investigate the loop-level constraints and focus on cLFV processes first. We stress that the non- λ' NP contributions to these decays, e.g. $\tau \rightarrow \ell\gamma$, $\mu \rightarrow e\gamma$, $\tau \rightarrow \ell'(\ell)\ell\ell$ ($\ell' \neq \ell$) and $\mu \rightarrow eee$, can be eliminated for the particular structure of (s)neutrino mass matrices, that is, only chiral mixing but no flavor mixing exists for the neutrino sector, when involving RH neutrinos, and the sneutrino sector (see e.g. Ref. [27]). Then, we focus on the λ' contributions

Observations	SM predictions	Experimental data
$\mathcal{B}(K^+ \rightarrow \pi^+ \nu \bar{\nu})$	$(9.24 \pm 0.83) \times 10^{-11}$ [76]	$(1.7 \pm 1.1) \times 10^{-10}$ [75]
$\mathcal{B}(B^+ \rightarrow K^+ \nu \bar{\nu})$	$(4.6 \pm 0.5) \times 10^{-6}$ [79]	$(1.1 \pm 0.4) \times 10^{-5}$ [77]
$\mathcal{B}(B \rightarrow K^{*0} \nu \bar{\nu})$	$(9.2 \pm 1.0) \times 10^{-6}$ [73]	$< 2.7 \times 10^{-5}$ [78]
$\mathcal{B}(D^0 \rightarrow \mu^+ \mu^-)$	$\lesssim 6 \times 10^{-11}$ [81]	$< 6.2 \times 10^{-9}$ [81]
$\mathcal{B}(\tau \rightarrow \mu \rho^0)$	-	$< 1.2 \times 10^{-8}$ [75]
$\mathcal{B}(B \rightarrow \tau \nu)$	$(9.47 \pm 1.82) \times 10^{-5}$ [82]	$(1.09 \pm 0.24) \times 10^{-4}$ [75]
$\mathcal{B}(D_s \rightarrow \tau \nu)$	$(5.40 \pm 0.30)\%$ [28]	$(5.48 \pm 0.23)\%$ [75]
$\mathcal{B}(\tau \rightarrow K \nu)$	$(7.15 \pm 0.026) \times 10^{-3}$ [83]	$(6.96 \pm 0.10) \times 10^{-3}$ [75]

Table 1: Current status of the related processes, which can be affected by RPV-MSSMIS at tree level. The experimental upper limits are given at 90% CL.

to the cLFV decays. The branching fraction of the $\tau \rightarrow \ell \gamma$ decay is given by

$$\mathcal{B}(\tau \rightarrow \ell \gamma) = \frac{\tau_\tau \alpha m_\tau^5}{4} (|A_2^L|^2 + |A_2^R|^2), \quad (3.6)$$

where the effective couplings $A_2^L = -\frac{\lambda'_{\ell j3} \lambda'_{3 j3}}{64\pi^2 m_{\tilde{b}_R}^2}$ and $A_2^R = 0$. The limit of m_ℓ^2/m_τ^2 is adopted here and also for other cLFV processes. It is worth noting that one of the cLFV muon decays, $\mu \rightarrow e \gamma$ constrains the coupling product $|\lambda'_{1j3} \lambda'_{2j3}|$ with a TeV scale $m_{\tilde{b}_R}$ very strongly for the experimental upper limit $\mathcal{B}(\mu \rightarrow e \gamma)_{\text{exp}} < 4.2 \times 10^{-13}$ at 90% CL [75]. That is, simultaneous large λ'_{1j3} and λ'_{2j3} are not favored, and hence it is also a reason for only non-negligible λ'_{1j3} or λ'_{2j3} considered at a time in this work. Then $\mu \rightarrow e \gamma$, $\mu \rightarrow eee$ and $\tau \rightarrow \ell^{(\prime)} \ell \ell$ will not be taken into consideration. The remained cLFV processes to be considered are $\tau \rightarrow \mu \gamma$, $\tau \rightarrow e \gamma$, $\tau \rightarrow \mu \mu \mu$ and $\tau \rightarrow eee$ decays (see the relevant formulas in Ref. [28]), with the experimental upper limits $\mathcal{B}(\tau \rightarrow \mu \gamma)_{\text{exp}} < 4.2 \times 10^{-8}$, $\mathcal{B}(\tau \rightarrow e \gamma)_{\text{exp}} < 3.3 \times 10^{-8}$, $\mathcal{B}(\tau \rightarrow \mu \mu \mu)_{\text{exp}} < 2.1 \times 10^{-8}$ and $\mathcal{B}(\tau \rightarrow eee)_{\text{exp}} < 2.7 \times 10^{-8}$ at 90% CL, respectively [75]².

Next we investigate the B -meson processes related to the FCNC. The $B_s - \bar{B}_s$ mixing is mastered by

$$\mathcal{L}_{\text{eff}}^{b\bar{s}b\bar{s}} = (C_{B_s}^{\text{SM}} + C_{B_s}^{\text{NP}})(\bar{s}\gamma_\mu P_L b)(\bar{s}\gamma^\mu P_L b) + \text{h.c.}, \quad (3.7)$$

where the SM contribution is $C_{B_s}^{\text{SM}} = -\frac{1}{4\pi^2} G_F^2 m_W^2 \eta_t^2 S(x_t)$ with the defined function $S(x_t) \equiv$

²In this work, in order to consider all the process constraints at 2σ level, we get the experiment bound $\mathcal{B}(\tau \rightarrow \mu \gamma)_{\text{exp}} < 5.1 \times 10^{-8}$, $\mathcal{B}(\tau \rightarrow e \gamma)_{\text{exp}} < 4 \times 10^{-8}$, $\mathcal{B}(\tau \rightarrow \mu \mu \mu)_{\text{exp}} < 2.6 \times 10^{-8}$, $\mathcal{B}(\tau \rightarrow eee)_{\text{exp}} < 3.3 \times 10^{-8}$ as well as $R_{K^*}^{\nu\bar{\nu}} < 3.3$ under the assumption that the uncertainties follow the Gaussian distribution [84].

$\frac{x_t(4-11x_t+x_t^2)}{4(x_t-1)^2} + \frac{3x_t^3 \log(x_t)}{2(x_t-1)^3}$, and the non-negligible NP contribution is,

$$C_{B_s}^{\text{NP}} = \frac{1}{8i} \left(\Lambda_{vv'}^{\mathcal{I}} D_2[m_{\tilde{\nu}_v^{\mathcal{I}}}, m_{\tilde{\nu}_{v'}^{\mathcal{I}}}, m_b, m_b] + \Lambda_{vv'}^{\mathcal{N}} D_2[m_{\nu_v}, m_{\nu_{v'}}, m_{\tilde{b}_R}, m_{\tilde{b}_R}] \right), \quad (3.8)$$

where $\Lambda_{vv'}^{\mathcal{I}} \equiv \lambda_{v33}^{\mathcal{I}} \lambda_{v23}^{\mathcal{I}*} \lambda_{v'33}^{\mathcal{I}} \lambda_{v'23}^{\mathcal{I}*}$ and $\Lambda_{vv'}^{\mathcal{N}} \equiv \lambda_{v33}^{\mathcal{N}} \lambda_{v23}^{\mathcal{N}*} \lambda_{v'33}^{\mathcal{N}} \lambda_{v'23}^{\mathcal{N}*}$. The recently updated measurement by LHCb, combined with previous ones, induces $\Delta M_s^{\text{LHCb}} = (17.7656 \pm 0.0057) \text{ ps}^{-1}$ [85]³, along with the SM prediction $\Delta M_s^{\text{SM}} = (18.4_{-1.2}^{+0.7}) \text{ ps}^{-1}$ [87], leads to the strong constraint,

$$0.90 < |1 + C_{B_s}^{\text{NP}}/C_{B_s}^{\text{SM}}| < 1.11, \quad (3.9)$$

at 2σ level.

Following the introduction of $B_s - \bar{B}_s$ mixing, we will mention the $B \rightarrow X_s \gamma$ decay, which are mastered by the electromagnetic dipole operator $\mathcal{O}_7 = \frac{m_b}{e} (\bar{s} \sigma^{\mu\nu} P_R b) F_{\mu\nu}$. The λ' contribution is given by

$$\Delta C_7^{\lambda'} = \frac{\sqrt{2} \lambda_{v3k}^{\mathcal{I}} \lambda_{v2k}^{\mathcal{I}*}}{144 G_F \eta_t m_{\tilde{\nu}_v^{\mathcal{I}}}^2}. \quad (3.10)$$

The non- λ' ones can be referred to Ref. [88] and are predicted negligible for the decoupled \tilde{u}_i . In order to fulfil the bound from the recent measured branching ratio $\mathcal{B}(B \rightarrow X_s \gamma)_{\text{exp}} \times 10^4 = 3.43 \pm 0.21 \pm 0.07$ [89] and the SM prediction $\mathcal{B}(B \rightarrow X_s \gamma)_{\text{SM}} \times 10^4 = 3.36 \pm 0.23$ [90], Eq. (3.10) implies a cancellation within $\lambda_{v33}^{\mathcal{I}} \lambda_{v23}^{\mathcal{I}*}$ for the degenerate $m_{\tilde{\nu}}$. This cancellation is also benefit for avoiding the bounds of $B_s - \bar{B}_s$ mixing (see Eq. (3.8)).

Then we move on to the constraints from the purely leptonic decays of Z , W bosons and $\tau(\mu)$ leptons. The effective Lagrangian of $Z \rightarrow l_i^- l_j^+$ decay is given by

$$\mathcal{L}_{\text{eff}}^{Zll} = \frac{e}{\cos \theta_W \sin \theta_W} \bar{l}_i \gamma^\mu (g_{l_L}^{ij} P_L + g_{l_R}^{ij} P_R) l_j Z_\mu, \quad (3.11)$$

where $g_{l_L}^{ij} = \delta^{ij} g_{l_L}^{\text{SM}} + \delta g_{l_L}^{ij}$ and $g_{l_R}^{ij} = \delta^{ij} g_{l_R}^{\text{SM}} + \delta g_{l_R}^{ij}$, with $g_{l_L}^{\text{SM}} = -\frac{1}{2} + \sin^2 \theta_W$ and $g_{l_R}^{\text{SM}} = \sin^2 \theta_W$. The NP effective couplings, contributed mainly by λ' effects, can be expressed as $\delta g_{l_L}^{ij} = \frac{1}{32\pi^2} B^{ij}$ ($\delta g_{l_R}^{ij} = 0$) and the formulas of B^{ij} functions are collected in the appendix C. The measurements of the partial width ratios of Z bosons, i.e. $\Gamma(Z \rightarrow \mu\mu)/\Gamma(Z \rightarrow ee) = 1.0001(24)$, $\Gamma(Z \rightarrow$

³This combined result by LHCb, is very close to the very recent result averaged by HFLAV, as $\Delta M_s^{\text{HFLAV-2021}} = (17.765 \pm 0.006) \text{ ps}^{-1}$ [86], with the much improved precision compared to the previous average, $\Delta M_s^{\text{HFLAV-2018}} = (17.757 \pm 0.021) \text{ ps}^{-1}$ [8].

Parameters	Sets	Parameters	Sets
$\tan \beta$	15	Y_ν	diag(0.41, 0.11, 0.10)
M_1	320 GeV	M_R	diag(1, 1, 1) TeV
M_2	350 GeV	B_{M_R}	diag(0.5, 0.5, 0.5) TeV ²
μ	450 GeV	$m_{\tilde{L}'_i}$	diag(360, 350, 350) GeV

Table 2: The sets of fixed model parameters, defined at μ_{NP} scale.

$\tau\tau)/\Gamma(Z \rightarrow \mu\mu) = 1.0010(26)$ and $\Gamma(Z \rightarrow \tau\tau)/\Gamma(Z \rightarrow ee) = 1.0020(32)$ [75], induce that $|B^{11}| < 0.36$ with $|B^{33}| < 0.32$ when $\lambda'_{2jk} = 0$ (Case A) and $|B^{22}| < 0.35$ with $|B^{33}| < 0.31$ when $\lambda'_{1jk} = 0$ (Case B). Here the additional dependence on η and h' in $g_{L(R)}$ through θ_W is omitted.

As for the constraints from the purely leptonic decays of W , they can be covered by the stronger ones from $\tau \rightarrow \ell \bar{\nu}_\ell \nu_\tau$ and $\mu \rightarrow e \bar{\nu}_e \nu_\mu$ decays. The measurements of the latter ones provide the bounds on model parameters [54], which can be expressed as

$$\begin{aligned}
\frac{1 + \eta_{\mu\mu} + \delta^{\text{BX}} h'_{\mu\mu}}{1 + \eta_{ee} + \delta^{\text{AX}} h'_{ee}} &= 1.0018(14), \\
\frac{1 + \eta_{\tau\tau} + h'_{\tau\tau}}{1 + \eta_{\mu\mu} + \delta^{\text{BX}} h'_{\mu\mu}} &= 1.0010(14), \\
\frac{1 + \eta_{\tau\tau} + h'_{\tau\tau}}{1 + \eta_{ee} + \delta^{\text{AX}} h'_{ee}} &= 1.0029(14),
\end{aligned} \tag{3.12}$$

where X is A(B) for Case A(B). Especially with the last two formulas of Eq. (3.12) combined with $|\eta_{\mu\mu}(h'_{\mu\mu})| \lesssim 10^{-4}$, we should keep $|\eta_{\tau\tau} + h'_{\tau\tau}| \lesssim 0.0018$ and $|\eta_{\tau\tau} + h'_{\tau\tau}| \lesssim |\eta_{ee} + \delta^{\text{AX}} h'_{ee}|$ at 2σ level, respectively.

4 Numerical analyses

In this section, we begin to study the numerical explanations for B -physics anomalies, $(g-2)_\mu$ and m_W shift in RPV-MSSMIS. With the data of neutrino oscillation [91], we consider normal ordering and zero δ_{CP} . Then the three light neutrinos have masses $\{0, 0.008, 0.05\}$ eV with $m_{\nu_i} \approx \text{diag}(0, \sqrt{\Delta m_{21}^2}, \sqrt{\Delta m_{31}^2})$ [92]. The sets of fixed model parameters are collected in table 2. The diagonal inputs of Y_ν , M_R , $m_{\tilde{L}'}$, $m_{\tilde{R}'}$, B_{M_R} and A_ν here induce no flavor mixings in sneutrino sector and the neutrino sector (when RH neutrinos engage), which are benefit for fulfilling the bounds of cLFV decays (see the appendix B for the particular discussions). Besides,

the input values shown in table 2 can induce a diagonal $\eta = -\text{diag}(2.53, 0.18, 0.15) \times 10^{-3}$. The values of $m_{\tilde{L}'_i}$ induce $m_{\tilde{\nu}_1(\tilde{l}_1)} = 348(352)$ GeV, which are larger than the masses of the lightest neutralino and chargino, as 307 GeV and 325 GeV, respectively, and they are in accord with the constraints discussed in section 3.1. The remained parameters, $m_{\tilde{b}_R}$, λ'_{323} , λ'_{333} , $\lambda'_{1(2)23}$ and $\lambda'_{1(2)33}$ in Case A (B), can vary freely in the ranges considered.

Next, with the input values given above and all λ' couplings as real, we can get some numerical results of Wilson coefficients and observables which show the possibilities for simultaneous explanations of the anomalies. They are given as follows,

$$\begin{aligned}\Delta C_{9\ell} &= -\Delta C_{10\ell} \approx -1.604(-1.623)\lambda'_{1(2)23}\lambda'_{1(2)33}, \\ C_{B_s}^{\text{NP}}/C_{B_s}^{\text{SM}} &\approx 76(\lambda'_{\ell 23}\lambda'_{\ell 33} + \lambda'_{323}\lambda'_{333})^2, \\ B^{33} &\approx \frac{1 \text{ TeV}^2}{m_{\tilde{b}_R}^2} [0.146 \log(m_{\tilde{b}_R}/1 \text{ TeV}) + 0.2] \lambda_{333}^{\prime 2},\end{aligned}\tag{4.1}$$

where only the dominant parts are kept. To be favored by the $R_{K^{(*)}}$ data at 2σ level, there are $-0.355 \lesssim \lambda'_{123}\lambda'_{133} \lesssim -0.106$ in Case A and $0.117 \lesssim \lambda'_{223}\lambda'_{233} \lesssim 0.314$ in Case B, through the first formula of Eq. (4.1), which is induced by Eq. (2.8). As for the second formula within Eq. (4.1), valid for $1.5 \leq m_{\tilde{b}_R} \leq 10$ TeV, we get $|\lambda'_{\ell 23}\lambda'_{\ell 33} + \lambda'_{323}\lambda'_{333}| \lesssim 0.038$ with Eq. (3.9). This result implies that the $B_s - \bar{B}_s$ mixing bound demands the cancelling between $\lambda'_{\ell 23}\lambda'_{\ell 33}$ and $\lambda'_{323}\lambda'_{333}$. In the last formula, the edge value of λ'_{333} near the $Z \rightarrow \tau^- \tau^+$ bound can be gotten. With the rough NP features for B -physics anomalies shown above, we will study them in details.

In Case A, we can see that the $R_{K^{(*)}}$ and $R_{D^{(*)}}$ anomalies can be simultaneously explained at 2σ level, although the overlaps are narrow, as shown in figure 1. The dominant constraints are from $B \rightarrow K^{(*)}\nu\bar{\nu}$, Z leptonic decays, $\tau \rightarrow eee$ decays and $B_s - \bar{B}_s$ mixing. In figure 1(a), when λ' couplings except λ'_{133} are fixed as shown in the figure, the lower limit of $m_{\tilde{b}_R}$ is constrained by the Z leptonic decays, i.e. $Z \rightarrow \tau^- \tau^+$ specifically, while \tilde{b}_R should also be lighter than around 2.42 TeV here to explain the $R_{D^{(*)}}$ data. Accordingly, the favored region for $R_{K^{(*)}}$ explanations are broad and is nearly independent of $m_{\tilde{b}_R}$ and only demands $\lambda'_{133} \gtrsim 1$ here. In figure 1(b), we set $\lambda'_{133} = 1.12$ and decrease $|\lambda'_{123}|$ slightly, and the contributions involving $m_{\tilde{b}_R}$ cannot be omitted because the chargino-sneutrino one is weakened slightly. The values of $(m_{\tilde{b}_R}, \lambda'_{333})$ in the overlap get smaller, then we can get $-h'_{ee} = 3.6 \times 10^{-4}$. The NP prediction m_W^{NP} without pure-MSSM effects is given by $m_W^{\text{NP}} \approx m_W^{\text{SM}}[1 - 0.20(\eta_{ee} + \eta_{\mu\mu} + h'_{ee})]$ (similar to

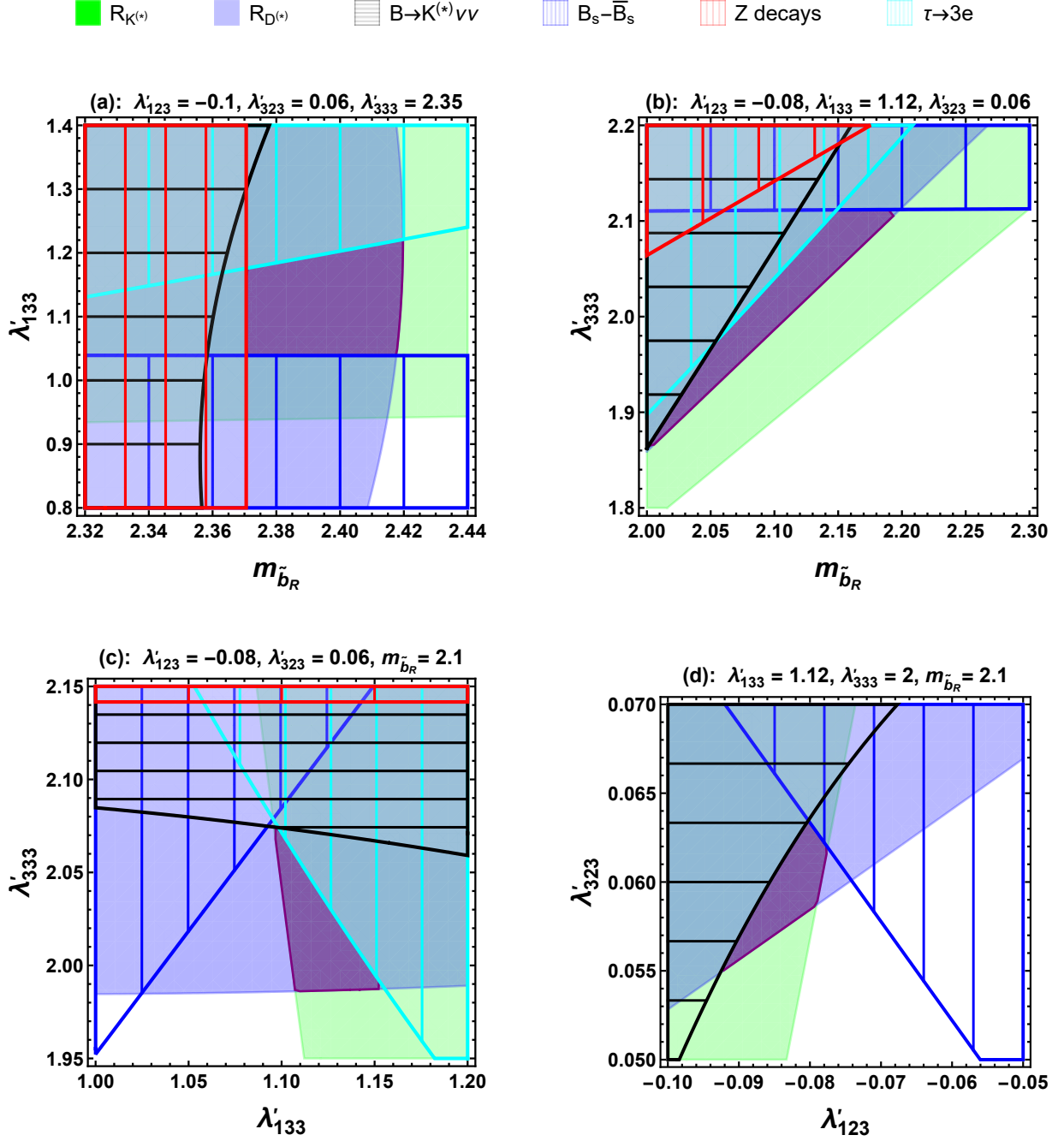


Figure 1: The experimental allowed regions for explaining the $R_{K^{(*)}}$ and $R_{D^{(*)}}$ anomalies in Case A. The masses $m_{\tilde{b}_R}$ are given in units of TeV. The 2σ favored areas for $R_{K^{(*)}}$ and $R_{D^{(*)}}$ measurements are denoted by green and blue, respectively. The hatched areas filled with the black-horizontal, red-vertical, cyan-vertical and blue-vertical lines are excluded at 2σ level, by the $B \rightarrow K^{(*)} \nu \bar{\nu}$, $Z \rightarrow l_i^- l_j^+$, $\tau \rightarrow eee$ decays and $B_s - \bar{B}_s$ mixing, respectively. The common areas are denoted by purple.

[59]), inducing the value $m_W^{\text{NP}} = 80.4124$ GeV, which can explain the CDF-II measurement at 2σ level. Keeping the values of $\lambda'_{123} = -0.08$ and $m_{\tilde{b}_R} = 2.1$ TeV, relevant overlaps are also found in figure 1(c) and figure 1(d).

Then we move onto the Case B. In this case, we will show that, given the stringent bounds from the $B_s - \bar{B}_s$ mixing as well as the constraints of $Z \rightarrow \tau^- \tau^+$ decay, $R_{K^{(*)}}$ and $R_{D^{(*)}}$ anomalies cannot be explained simultaneously at 2σ level. From Eqs. (2.11)-(2.12), ones can see that the $R_{D^{(*)}}$ data explanation favors large $|\lambda'_{333}|$, positive $\lambda'_{323}\lambda'_{333}$ and negative $\lambda'_{223}\lambda'_{233}$. However, positive $\lambda'_{223}\lambda'_{233}$ is needed for explaining $R_{K^{(*)}}$. Thus, with Eq. (4.1), we let λ'_{223} be the edge value $0.117/\lambda'_{233}$ for $R_{K^{(*)}}$ explanations and $\lambda'_{323} = (-0.117 + 0.038)/\lambda'_{333}$ for the bound edge of $B_s - \bar{B}_s$ mixing, with $\lambda'_{333} = \sqrt{0.31}(m_{\tilde{b}_R}/1 \text{ TeV}) / [0.146 \log(m_{\tilde{b}_R}/1 \text{ TeV}) + 0.2]^{\frac{1}{2}}$ as the edge value near the $Z \rightarrow \tau^- \tau^+$ bound. Then the approximate prediction of $\mathcal{R}_{D^{(*)}}^{\text{NP/SM}}$ can be given as the function of $(m_{\tilde{b}_R}, \lambda'_{233})$, as shown in figure 2. We find that for $0.5 \lesssim \lambda'_{233} \lesssim 1$, the

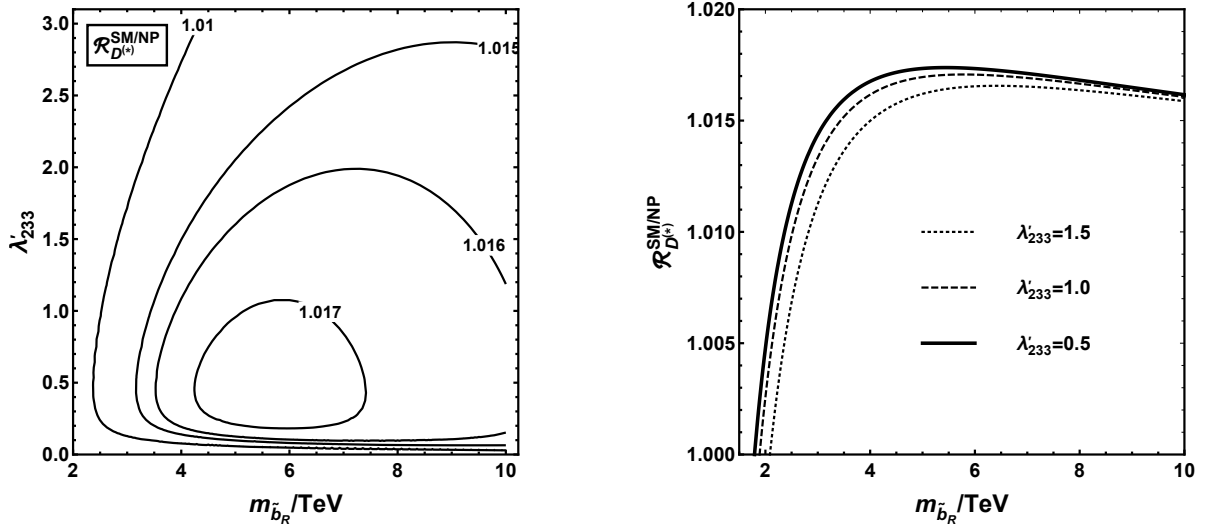


Figure 2: The ratio $\mathcal{R}_{D^{(*)}}^{\text{NP/SM}}$ varies with $m_{\tilde{b}_R}$ and λ'_{233} in Case B. In the right panel, λ'_{233} is set as 1.5 (dotted), 1 (dashed) and 0.5 (solid), respectively.

ratio increases with $m_{\tilde{b}_R}$ increasing up to around 6 TeV, due to the edge value of λ'_{333} getting relative large for heavier $m_{\tilde{b}_R}$ in this range. Then the ratio decreases for $m_{\tilde{b}_R} \gtrsim 6$ TeV. From the right panel of figure 2, it is obvious that $\mathcal{R}_{D^{(*)}}^{\text{NP/SM}}$ cannot be raised higher than 1.02, with below the lower limit 1.05 of 2σ fit. Thus, the simultaneous 2σ -level explanation of $R_{K^{(*)}}$ and $R_{D^{(*)}}$ anomalies is impossible in Case B. While we can still explain $R_{K^{(*)}}$ and other anomalies in the $b \rightarrow s\mu^+\mu^-$ process, which will be shown in table 3, with the benchmark point in Case A collected as well.

In table 3, as mentioned before, for the point in Case A, both $R_{K^{(*)}}$ and $R_{D^{(*)}}$ are in the 2σ ranges of the experimental measurements. In Case B(I), we utilize the relevant point to fulfil the $R_{K^{(*)}}$ data at 2σ , and raise the ratio $\mathcal{R}_{D^{(*)}}^{\text{NP/SM}}$. However, this increase cannot reach the 2σ accordance region as we predicted. The Case B(II) point can explain the $b \rightarrow s\ell^+\ell^-$ anomalies at 2σ level without considering the $R_{D^{(*)}}$ data. Besides, in all the three cases, the $(g-2)_\mu$ data and CDF-II m_W shift favor the points, which allowed by relevant constraints shown in section 3. Due to the contributions of λ' diagrams, there are slight differences among the predicted δa_μ^{NP} in the three cases. We mention that, in case the CDF-II result is not supported by the future measurements, we can also adjust the coupling Y_ν in table 2 into, e.g. $\text{diag}(0.12, 0.11, 0.10)$, which induces $\eta_{ee} = -2.2 \times 10^{-4}$ to fulfil the current global $m_W = 80.379(12)$ GeV [75] and relevant measurements of $\sin\theta_W$ mentioned in section 2.4. We have checked that the explanations for the other anomalies in Case A, Case B(I) and Case B(II) are still applicable. Besides, this model framework predicts the heavy neutrinos with the TeV scale masses, which reach the searches of future collider [93, 94].

	Case A	Case B(I)	Case B(II)
$\lambda'_{\ell 23}$	-0.08	0.1	0.1
$\lambda'_{\ell 33}$	1.12	1.35	2
λ'_{323}	0.06	-0.04	-0.1
λ'_{333}	2	2.6	2
$m_{\tilde{b}_R}/\text{TeV}$	2.1	3	3
$\Delta C_{9\ell} = -\Delta C_{10\ell}$	0.172	-0.196	-0.295
C_9^{U}	-0.157	-0.158	-0.001
$\mathcal{R}_{D^{(*)}}^{\text{NP/SM}}$	1.055	1.006	0.983
$m_W^{\text{NP}}/\text{GeV}$	80.412	80.411	80.416
$\delta a_\mu^{\text{NP}} \times 10^9$	1.361	1.369	1.377

Table 3: The benchmark points in Case A ($\ell = 1$ and e) and B ($\ell = 2$ and μ). The Wilson coefficient C_9^{U} provides the lepton flavor universal contribution.

5 Conclusions

The recent reported anomalies in $R_{D^{(*)}}$, $R_{K^{(*)}}$ within $b \rightarrow s\ell^+\ell^-$ observables, e.g. P'_5 , $\mathcal{B}(B_s \rightarrow \phi\mu^+\mu^-)$, as well as the enduring muon $g-2$, have shown the LFUV effects beyond SM may exist. While the more recent precision measurement of W mass, if confirmed by other experiments,

will profoundly change the situation of NP search. Interestingly, the LFUV NP can effect m_W prediction through muon decays, so it is straightforward to make a simultaneous investigation on the B -physics anomalies, $(g-2)_\mu$ and m_W in the NP models.

In this work, we study these anomalies mentioned above in RPV-MSSMIS, which is the framework providing $\lambda' \hat{L} \hat{Q} \hat{D}$ interaction involved with the (s)neutrino chiral mixing for explaining B -physics anomalies and increasing m_W prediction, which is also contributed by the non-unitarity η_{ee} in the seesaw sector. We consider $\lambda'_{1(2)jk}$ nonzero at a time in Case A(B), and find the deviations of $R_{K^{(*)}}$, $R_{D^{(*)}}$, and m_W from SM predictions can be reduced to 2σ level simultaneously in Case A. In Case B, the combined 2σ -level explanation of $b \rightarrow s\ell^+\ell^-$ anomaly and m_W -shift can be achieved, while NP effects on $R_{D^{(*)}}$ is weak. Moreover, the $(g-2)_\mu$ data and m_W -shift can be explained in both cases, which also fulfil neutrino oscillation data, the relevant constraints at collider and series of flavor-physics bounds from $B \rightarrow K^{(*)}\nu\bar{\nu}$, Z leptonic decays, cLFV decays, $B_s - \bar{B}_s$ mixing, etc.

Acknowledgements

This work is supported in part by the National Natural Science Foundation of China under Grant No. 11875327, the Fundamental Research Funds for the Central Universities, and the Sun Yat-Sen University Science Foundation. F.C. is also supported by the CCNU-QLPL Innovation Fund (QLPL2021P01).

A One-loop box contributions to $b \rightarrow s\ell^+\ell^-$ in RPV-MSSMIS

In this section, the whole Wilson coefficients from the one-loop $b \rightarrow s\ell^+\ell^-$ boxes in RPV-MSSMIS are listed.

The LH-quark-current contributions from chargino boxes to $b \rightarrow s\ell^+\ell^-$ process are given by,

$$\begin{aligned} \Delta C_{9\ell}^{\chi^\pm} = -\Delta C_{10\ell}^{\chi^\pm} = & -\frac{\sqrt{2}\pi^2 i}{2G_F\eta_t e^2} \left(g_2^2 K_{i3} K_{i2}^* V_{m1}^* V_{n1} (g_2 V_{m1} \tilde{\mathcal{V}}_{v\ell}^{\mathcal{I}} - V_{m2} Y_{\ell v}^{\mathcal{I}}) \right. \\ & (g_2 V_{n1}^* \tilde{\mathcal{V}}_{v\ell}^{\mathcal{I}} - V_{n2}^* Y_{\ell v}^{\mathcal{I}}) D_2[m_{\tilde{\nu}_v^{\mathcal{I}}}, m_{\chi_m^\pm}, m_{\chi_n^\pm}, m_{\tilde{u}_{Li}}] \\ & \left. + y_{u_i}^2 K_{i3} K_{i2}^* V_{m2}^* V_{n2} (g_2 V_{m1} \tilde{\mathcal{V}}_{v\ell}^{\mathcal{I}} - V_{m2} Y_{\ell v}^{\mathcal{I}}) \right) \end{aligned}$$

$$\begin{aligned}
& (g_2 V_{n1}^* \tilde{\mathcal{V}}_{v\ell}^{\mathcal{I}} - V_{n2}^* Y_{\ell v}^{\mathcal{I}}) D_2[m_{\tilde{\nu}_v^{\mathcal{I}}}, m_{\chi_m^\pm}, m_{\chi_n^\pm}, m_{\tilde{u}_{Ri}}] \\
& - \lambda_{v3k}^{\mathcal{I}} \lambda_{v'2k}^{\mathcal{I}*} (g_2 V_{m1}^* \tilde{\mathcal{V}}_{v\ell}^{\mathcal{I}} - V_{m2}^* Y_{\ell v}^{\mathcal{I}}) (g_2 V_{m1} \tilde{\mathcal{V}}_{v'\ell}^{\mathcal{I}} - V_{m2} Y_{\ell v'}^{\mathcal{I}}) D_2[m_{\tilde{\nu}_v^{\mathcal{I}}}, m_{\tilde{\nu}_{v'}^{\mathcal{I}}}, m_{\chi_m^\pm}, m_{d_k}] \\
& - \tilde{\lambda}'_{\ell ik} \tilde{\lambda}_{\ell jk}^{\mathcal{I}*} g_2^2 K_{i3} K_{j2}^* |V_{m1}|^2 D_2[m_{\tilde{u}_{Li}}, m_{\tilde{u}_{Lj}}, m_{\chi_m^\pm}, m_{d_k}] \\
& + \tilde{\lambda}'_{\ell ik} \lambda_{v2k}^{\mathcal{I}*} (g_2 K_{i3} V_{m1}^*) (g_2 V_{m1} \tilde{\mathcal{V}}_{v\ell}^{\mathcal{I}} - V_{m2} Y_{\ell v}^{\mathcal{I}}) D_2[m_{\tilde{\nu}_v^{\mathcal{I}}}, m_{\tilde{u}_{Li}}, m_{\chi_m^\pm}, m_{d_k}] \\
& + \tilde{\lambda}_{\ell ik}^{\mathcal{I}*} \lambda_{v3k}^{\mathcal{I}} (g_2 K_{i2}^* V_{m1}) (g_2 V_{m1}^* \tilde{\mathcal{V}}_{v\ell}^{\mathcal{I}} - V_{m2}^* Y_{\ell v}^{\mathcal{I}}) D_2[m_{\tilde{\nu}_v^{\mathcal{I}}}, m_{\tilde{u}_{Li}}, m_{\chi_m^\pm}, m_{d_k}] \Big), \tag{A.1}
\end{aligned}$$

where the Yukawa coupling $y_{u_i} = \sqrt{2}m_{u_i}/v_u$ and $Y_{\ell v}^{\mathcal{I}} = (Y_\nu)_{j\ell} \tilde{\mathcal{V}}_{v(j+3)}^{\mathcal{I}*}$. While the corresponding RH-quark-current contributions are,

$$\begin{aligned}
\Delta C_{9\ell}'^{\chi^\pm} &= -\Delta C_{10\ell}'^{\chi^\pm} = -\frac{\sqrt{2}\pi^2 i}{2G_F \eta_t e^2} \lambda_{vi2}^{\mathcal{I}} \lambda_{v'i3}^{\mathcal{I}*} (g_2 V_{m1}^* \tilde{\mathcal{V}}_{v\ell}^{\mathcal{I}} - V_{m2}^* Y_{\ell v}^{\mathcal{I}}) \\
& (g_2 V_{m1} \tilde{\mathcal{V}}_{v'\ell}^{\mathcal{I}} - V_{m2} Y_{\ell v'}^{\mathcal{I}}) D_2[m_{\tilde{\nu}_v^{\mathcal{I}}}, m_{\tilde{\nu}_{v'}^{\mathcal{I}}}, m_{\chi_m^\pm}, m_{d_i}]. \tag{A.2}
\end{aligned}$$

The contributions of W/H^\pm (means W with W Goldstones or charged Higgs box involved) box diagrams to $b \rightarrow s\ell^+\ell^-$ process are given by,

$$\begin{aligned}
\Delta C_{9\ell}^{W/H^\pm} &= -\Delta C_{10\ell}^{W/H^\pm} = -\frac{\sqrt{2}\pi^2 i}{2G_F \eta_t e^2} \Big(y_{u_i}^2 K_{i3} K_{i2}^* Z_{H_{h2}}^2 Z_{H_{h'2}}^2 |Y_{\ell v}^{\mathcal{N}}|^2 D_2[m_{\nu_v}, m_{u_i}, m_{H_h}, m_{H_{h'}}] \\
& - 4g_2^2 m_{u_i} y_{u_i} m_{\nu_v} K_{i3} K_{i2}^* Z_{H_{h2}}^2 \text{Re}(\mathcal{V}_{v\ell}^* Y_{\ell v}^{\mathcal{N}*}) D_0[m_{\nu_v}, m_{u_i}, m_W, m_{H_h}] \\
& + 5g_2^4 K_{i3} K_{i2}^* |\mathcal{V}_{v\ell}^*|^2 D_2[m_{\nu_v}, m_{u_i}, m_W, m_W] \\
& + Z_{H_{h2}}^2 Y_{\ell v}^{\mathcal{N}*} Y_{\ell v'}^{\mathcal{N}} \lambda_{v3k}^{\mathcal{N}} \lambda_{v'2k}^{\mathcal{N}*} D_2[m_{\nu_v}, m_{\nu_{v'}}, m_{H_h}, m_{\tilde{d}_{Rk}}] \\
& - 2g_2^2 m_{\nu_v} m_{\nu_{v'}} \mathcal{V}_{v\ell} \mathcal{V}_{v'\ell}^* \lambda_{v3k}^{\mathcal{N}} \lambda_{v'2k}^{\mathcal{N}*} D_0[m_{\nu_v}, m_{\nu_{v'}}, m_W, m_{\tilde{d}_{Rk}}] \\
& + 2m_{\nu_v} m_{\nu_{v'}} Z_{H_{h2}}^2 Y_{\ell v}^{\mathcal{N}} Y_{\ell v'}^{\mathcal{N}*} \lambda_{v3k}^{\mathcal{N}} \lambda_{v'2k}^{\mathcal{N}*} D_0[m_{\nu_v}, m_{\nu_{v'}}, m_{H_h}, m_{\tilde{d}_{Rk}}] \\
& + 2m_{u_i} m_{u_j} y_{u_i} y_{u_j} K_{i3} K_{j2}^* Z_{H_{h2}}^2 \tilde{\lambda}'_{\ell ik} \tilde{\lambda}_{\ell jk}^{\mathcal{I}*} D_0[m_{u_i}, m_{u_j}, m_{H_h}, m_{\tilde{d}_{Rk}}] \\
& - g_2^2 \mathcal{V}_{v\ell}^* \mathcal{V}_{v'\ell} \lambda_{v3k}^{\mathcal{N}} \lambda_{v'2k}^{\mathcal{N}*} D_2[m_{\nu_v}, m_{\nu_{v'}}, m_W, m_{\tilde{d}_{Rk}}] \\
& - g_2^2 K_{i3} K_{j2}^* \tilde{\lambda}'_{\ell ik} \tilde{\lambda}_{\ell jk}^{\mathcal{I}*} D_2[m_{u_i}, m_{u_j}, m_W, m_{\tilde{d}_{Rk}}] \\
& - 2m_{u_i} y_{u_i} m_{\nu_v} K_{i3} Z_{H_{h2}}^2 Y_{\ell v}^{\mathcal{N}*} \tilde{\lambda}'_{\ell ik} \lambda_{v2k}^{\mathcal{N}*} D_0[m_{u_i}, m_{\nu_v}, m_{H_h}, m_{\tilde{d}_{Rk}}] \\
& - 2m_{u_i} y_{u_i} m_{\nu_v} K_{i2}^* Z_{H_{h2}}^2 Y_{\ell v}^{\mathcal{N}} \tilde{\lambda}_{\ell ik}^{\mathcal{I}*} \lambda_{v3k}^{\mathcal{N}} D_0[m_{u_i}, m_{\nu_v}, m_{H_h}, m_{\tilde{d}_{Rk}}] \\
& + g_2^2 K_{i2}^* \mathcal{V}_{v\ell}^* \tilde{\lambda}_{\ell ik}^{\mathcal{I}*} \lambda_{v3k}^{\mathcal{N}} D_2[m_{u_i}, m_{\nu_v}, m_W, m_{\tilde{d}_{Rk}}] \\
& + g_2^2 K_{i3} \mathcal{V}_{v\ell} \tilde{\lambda}_{\ell ik}^{\mathcal{I}*} \lambda_{v2k}^{\mathcal{N}*} D_2[m_{u_i}, m_{\nu_v}, m_W, m_{\tilde{d}_{Rk}}] \Big), \tag{A.3}
\end{aligned}$$

$$\begin{aligned}
\Delta C_{9\ell}'^{W/H^\pm} &= -\Delta C_{10\ell}'^{W/H^\pm} = -\frac{\sqrt{2}\pi^2 i}{2G_F\eta_t e^2} \left(-2Z_{H_{h2}}^2 Y_{\ell v}^{\mathcal{N}*} Y_{\ell v'}^{\mathcal{N}} \lambda_{v'i2}^{\mathcal{N}} \lambda_{vi3}^{\mathcal{N}*} m_{\nu_v} m_{\nu_{v'}} \right. \\
&\quad \times D_0[m_{\nu_v}, m_{\nu_{v'}}, m_{H_h}, m_{\tilde{d}_{Li}}] - Z_{H_{h2}}^2 Y_{\ell v}^{\mathcal{N}} Y_{\ell v'}^{\mathcal{N}*} \lambda_{v'i2}^{\mathcal{N}} \lambda_{vi3}^{\mathcal{N}*} D_2[m_{\nu_v}, m_{\nu_{v'}}, m_{H_h}, m_{\tilde{d}_{Li}}] \\
&\quad + g_2^2 \mathcal{V}_{v\ell}^* \mathcal{V}_{v'\ell} \lambda_{v'i2}^{\mathcal{N}} \lambda_{v'i3}^{\mathcal{N}*} D_2[m_{\nu_v}, m_{\nu_{v'}}, m_W, m_{\tilde{d}_{Li}}] \\
&\quad \left. + 2g_2^2 \mathcal{V}_{v\ell}^* \mathcal{V}_{v'\ell} \lambda_{v'i2}^{\mathcal{N}} \lambda_{vi3}^{\mathcal{N}*} m_{\nu_v} m_{\nu_{v'}} D_0[m_{\nu_v}, m_{\nu_{v'}}, m_W, m_{\tilde{d}_{Li}}] \right), \tag{A.4}
\end{aligned}$$

where the mixing matrix elements $Z_{H_{12}} = -\sin\beta$, $Z_{H_{22}} = -\cos\beta$ with Goldstone mass $m_{H_1} = m_W$ and changed Higgs mass $m_{H_2} = m_{H^\pm}$ and $Y_{\ell v}^{\mathcal{N}} = (Y_\nu)_{j\ell} \mathcal{V}_{v(j+3)}$.

The contributions of $4\lambda'$ box diagrams to $b \rightarrow s\ell^+\ell^-$ process are given by,

$$\begin{aligned}
\Delta C_{9\ell}'^{4\lambda'} &= -\Delta C_{10\ell}'^{4\lambda'} = -\frac{\sqrt{2}\pi^2 i}{2G_F\eta_t e^2} \left(\tilde{\lambda}'_{\ell ik} \tilde{\lambda}_{\ell ik'}^* \lambda_{v3k'}^{\mathcal{N}} \lambda_{v2k}^{\mathcal{N}*} D_2[m_{\nu_v}, m_{u_i}, m_{\tilde{d}_{Rk}}, m_{\tilde{d}_{Rk'}}] \right. \\
&\quad \left. + \tilde{\lambda}'_{\ell ik'} \tilde{\lambda}_{\ell ik}^* \lambda_{v3k}^{\mathcal{N}} \lambda_{v2k'}^{\mathcal{N}*} D_2[m_{\tilde{\nu}_v}, m_{\tilde{u}_{Li}}, m_{d_k}, m_{d_{k'}}] \right), \tag{A.5}
\end{aligned}$$

$$\begin{aligned}
\Delta C_{9\ell}'^{4\lambda'} &= -\Delta C_{10\ell}'^{4\lambda'} = -\frac{\sqrt{2}\pi^2 i}{2G_F\eta_t e^2} \left(\tilde{\lambda}'_{\ell ij} \tilde{\lambda}_{\ell ij'}^* \lambda_{vj2}^{\mathcal{N}} \lambda_{vj'3}^{\mathcal{N}*} D_2[m_{\nu_v}, m_{u_i}, m_{\tilde{d}_{Lj}}, m_{\tilde{d}_{Lj'}}] \right. \\
&\quad \left. - \tilde{\lambda}'_{\ell j'k} \tilde{\lambda}_{\ell jk}^* \tilde{\lambda}'_{ij2} \tilde{\lambda}_{ij'3}^* (D_2[m_{l_i}, m_{\tilde{u}_{Lj}}, m_{\tilde{u}_{Lj'}}, m_{d_k}] + D_2[m_{\tilde{l}_{Li}}, m_{u_j}, m_{u_{j'}}, m_{\tilde{d}_{Rk}}]) \right). \tag{A.6}
\end{aligned}$$

The contributions of neutralino box diagrams only contain RH-quark-current parts, which are given by,

$$\begin{aligned}
\Delta C_{9\ell}'^{\chi^0} &= -\Delta C_{10\ell}'^{\chi^0} = -\frac{\sqrt{2}\pi^2 i}{2G_F\eta_t e^2} \left(\frac{1}{2} (g_1 N_{n1} + g_2 N_{n2})^2 \tilde{\lambda}'_{\ell i2} \tilde{\lambda}_{\ell i3}^* D_2[m_{\tilde{l}_{L\ell}}, m_{\tilde{l}_{L\ell}}, m_{u_i}, m_{\chi_n^0}] \right. \\
&\quad + \frac{2}{9} g_1^2 |N_{n1}|^2 \tilde{\lambda}'_{\ell i2} \tilde{\lambda}_{\ell i3}^* D_2[m_{u_i}, m_{\chi_n^0}, m_{\tilde{s}_R}, m_{\tilde{b}_R}] \\
&\quad - \frac{1}{3} N_{n1} g_1 (g_1 N_{n1} + g_2 N_{n2}) \tilde{\lambda}'_{\ell i2} \tilde{\lambda}_{\ell i3}^* \\
&\quad \left. \times (D_2[m_{\tilde{l}_{L\ell}}, m_{u_i}, m_{\chi_n^0}, m_{\tilde{s}_R}] + D_2[m_{\tilde{l}_{L\ell}}, m_{u_i}, m_{\chi_n^0}, m_{\tilde{b}_R}]) \right). \tag{A.7}
\end{aligned}$$

In the formulas above, the Passarino-Veltman functions [52] D_0 and D_2 are defined as,

$$D_0[m_1, m_2, m_3, m_4] \equiv \int \frac{d^4 k}{(2\pi)^4} \frac{1}{(k^2 - m_1^2)(k^2 - m_2^2)(k^2 - m_3^2)(k^2 - m_4^2)} \tag{A.8}$$

$$D_2[m_1, m_2, m_3, m_4] \equiv \int \frac{d^4 k}{(2\pi)^4} \frac{k^2}{(k^2 - m_1^2)(k^2 - m_2^2)(k^2 - m_3^2)(k^2 - m_4^2)} \tag{A.9}$$

B The numerical form of the (s)neutrino mixing matrix

With the input set in table 2, the numerical form of the neutrino mixing matrix is listed as

$$\mathcal{V}^T \approx \begin{pmatrix} 0.835 & 0.526 & -0.145 & 0.050i & 0 & 0 & -0.050 & 0 & 0 \\ -0.247 & 0.600 & 0.761 & 0 & 0.013i & 0 & 0 & 0.013 & 0 \\ 0.488 & -0.601 & 0.633 & 0 & 0 & 0.012i & 0 & 0 & -0.012 \\ 0 & 0 & 0 & 0.707i & 0 & 0 & -0.707 & 0 & 0 \\ 0 & 0 & 0 & 0 & 0.707i & 0 & 0 & 0.707 & 0 \\ 0 & 0 & 0 & 0 & 0 & 0.707i & 0 & 0 & -0.707 \\ -0.059 & -0.037 & 0.010 & 0.705i & 0 & 0 & -0.705 & 0 & 0 \\ 0.005 & -0.011 & -0.015 & 0 & 0.707i & 0 & 0 & 0.707 & 0 \\ -0.008 & 0.010 & -0.011 & 0 & 0 & 0.707i & 0 & 0 & -0.707 \end{pmatrix}, \quad (\text{B.1})$$

related to the neutrino mass spectrum $\text{diag}(0, 8 \times 10^{-15}, 5 \times 10^{-14}, 1, 1, 1, 1, 1, 1)$ TeV. And the sneutrino mixing matrix is given numerically by

$$\tilde{\mathcal{V}}^T \approx \begin{pmatrix} 0.991 & 0 & 0 & 0.067 & 0 & 0 & -0.118 & 0 & 0 \\ 0 & 0.999 & 0 & 0 & 0.018 & 0 & 0 & -0.032 & 0 \\ 0 & 0 & -0.999 & 0 & 0 & -0.017 & 0 & 0 & 0.029 \\ -0.131 & 0 & 0 & 0.704 & 0 & 0 & -0.698 & 0 & 0 \\ 0 & 0.036 & 0 & 0 & -0.707 & 0 & 0 & 0.706 & 0 \\ 0 & 0 & 0.032 & 0 & 0 & -0.707 & 0 & 0 & 0.707 \\ 0.037 & 0 & 0 & 0.707 & 0 & 0 & 0.706 & 0 & 0 \\ 0 & 0.010 & 0 & 0 & 0.707 & 0 & 0 & 0.707 & 0 \\ 0 & 0 & -0.009 & 0 & 0 & -0.707 & 0 & 0 & -0.707 \end{pmatrix}, \quad (\text{B.2})$$

related to the sneutrino mass spectrum $\text{diag}(348, 349, 349, 714, 708, 707, 1227, 1225, 1225)$ GeV.

Then one can find, all the chargino-sneutrino diagrams and the neutralino-slepton diagrams, among the non- λ' diagrams in the cLFV decays of leptons, make negligible contributions due to the vanishing of flavor mixing in sneutrino sector, as shown in Eq. (B.2), as well as the diagonal mass matrix of charged slepton for simplicity. As to W/H^\pm -neutrino diagrams, they are always

connected to terms $\mathcal{V}_{(\alpha+3)v}^{T*} \mathcal{V}_{(\beta+3)v}^T$, $\mathcal{V}_{(\alpha+3)v}^{T*} \mathcal{V}_{\beta v}^T$, $\mathcal{V}_{\alpha v}^{T*} \mathcal{V}_{\beta v}^T$ and conjugate terms ($\alpha, \beta = e, \mu, \tau$ and $\alpha \neq \beta$). Readers can see calculations of these diagrams in Ref. [95]. With the numerical form of Eq. (B.1), the $\mathcal{V}_{(\alpha+3)v}^{T*} \mathcal{V}_{(\beta+3)v}^T$ and $\mathcal{V}_{(\alpha+3)v}^{T*} \mathcal{V}_{\beta v}^T$ terms vanish. The $\mathcal{V}_{\alpha v}^{T*} \mathcal{V}_{\beta v}^T$ term can be decomposed into two parts, $\sum_{v_h=4}^9 \mathcal{V}_{\alpha v_h}^{T*} \mathcal{V}_{\beta v_h}^T$ and $\sum_{i=1}^3 \mathcal{V}_{\alpha i}^{T*} \mathcal{V}_{\beta i}^T = -\sum_{v_h=4}^9 \mathcal{V}_{\alpha v_h}^{T*} \mathcal{V}_{\beta v_h}^T$, related to the nearly degenerate heavy neutrinos and light neutrinos respectively [96]. Then one can also find that the $\mathcal{V}_{\alpha v}^{T*} \mathcal{V}_{\beta v}^T$ term makes no effective contribution to the cLFV decays of leptons. Thus, we conclude that the non- λ' diagrams provide negligible effects on the cLFV decays of leptons mentioned in section 3.3, in our input sets.

C The coupling functions in $Z \rightarrow l_i^- l_j^+$ process

With the effective Lagrangian of $Z \rightarrow l_i^- l_j^+$ process in Eq. (3.11) and the functions $B^{ij} \equiv (32\pi^2)\delta g_{l_L}^{ij}$ are given by the following two parts [80],

$$\begin{aligned} B_1^{ij} &= 3\tilde{\lambda}'_{j33}\tilde{\lambda}_{i33}^* \left\{ -x_{\tilde{b}_R}(1 + \log x_{\tilde{b}_R}) + \frac{m_Z^2}{18m_{\tilde{b}_R}^2} \left[(11 - 10\sin^2\theta_W) \right. \right. \\ &\quad \left. \left. + (6 - 8\sin^2\theta_W)\log x_{\tilde{b}_R} + \frac{1}{10}(-9 + 16\sin^2\theta_W)\frac{m_Z^2}{m_t^2} \right] \right\}, \\ B_2^{ij} &= \sum_{\ell=1}^2 \tilde{\lambda}'_{j\ell 3}\tilde{\lambda}_{i\ell 3}^* \frac{m_Z^2}{m_{\tilde{b}_R}^2} \left[\left(1 - \frac{4}{3}\sin^2\theta_W\right) \left(\log \frac{m_Z^2}{m_{\tilde{b}_R}^2} - i\pi - \frac{1}{3}\right) + \frac{\sin^2\theta_W}{9} \right]. \end{aligned} \quad (C.1)$$

Then there are $B^{ij} = B_1^{ij} + B_2^{ij}$, where the B_1^{ij} part is dominant due to the involved top quark.

References

- [1] **LHCb** Collaboration, R. Aaij et al., *Test of lepton universality in beauty-quark decays*, *Nature Phys.* **18** (2022), no. 3 277–282, [arXiv:2103.11769].
- [2] **LHCb** Collaboration, R. Aaij et al., *Test of lepton universality with $B^0 \rightarrow K^{*0} \ell^+ \ell^-$ decays*, *JHEP* **08** (2017) 055, [arXiv:1705.05802].
- [3] **LHCb** Collaboration, R. Aaij et al., *Measurement of CP-Averaged Observables in the $B^0 \rightarrow K^{*0} \mu^+ \mu^-$ Decay*, *Phys. Rev. Lett.* **125** (2020), no. 1 011802, [arXiv:2003.04831].

- [4] **LHCb** Collaboration, R. Aaij et al., *Branching Fraction Measurements of the Rare $B_s^0 \rightarrow \phi \mu^+ \mu^-$ and $B_s^0 \rightarrow f_2'(1525) \mu^+ \mu^-$ Decays*, *Phys. Rev. Lett.* **127** (2021), no. 15 151801, [[arXiv:2105.14007](#)].
- [5] **LHCb** Collaboration, R. Aaij et al., *Measurement of the $B_s^0 \rightarrow \mu^+ \mu^-$ decay properties and search for the $B^0 \rightarrow \mu^+ \mu^-$ and $B_s^0 \rightarrow \mu^+ \mu^- \gamma$ decays*, *Phys. Rev. D* **105** (2022), no. 1 012010, [[arXiv:2108.09283](#)].
- [6] **LHCb** Collaboration, R. Aaij et al., *Analysis of Neutral B-Meson Decays into Two Muons*, *Phys. Rev. Lett.* **128** (2022), no. 4 041801, [[arXiv:2108.09284](#)].
- [7] **CMS** Collaboration, A. M. Sirunyan et al., *Measurement of properties of $B_s^0 \rightarrow \mu^+ \mu^-$ decays and search for $B^0 \rightarrow \mu^+ \mu^-$ with the CMS experiment*, *JHEP* **04** (2020) 188, [[arXiv:1910.12127](#)].
- [8] **HFLAV** Collaboration, Y. S. Amhis et al., *Averages of b-hadron, c-hadron, and τ -lepton properties as of 2018*, *Eur. Phys. J. C* **81** (2021), no. 3 226, [[arXiv:1909.12524](#)].
- [9] **Muon g-2** Collaboration, B. Abi et al., *Measurement of the Positive Muon Anomalous Magnetic Moment to 0.46 ppm*, *Phys. Rev. Lett.* **126** (2021), no. 14 141801, [[arXiv:2104.03281](#)].
- [10] **Muon g-2** Collaboration, G. W. Bennett et al., *Final Report of the Muon E821 Anomalous Magnetic Moment Measurement at BNL*, *Phys. Rev. D* **73** (2006) 072003, [[hep-ex/0602035](#)].
- [11] T. Aoyama et al., *The anomalous magnetic moment of the muon in the Standard Model*, *Phys. Rept.* **887** (2020) 1–166, [[arXiv:2006.04822](#)].
- [12] S. Borsanyi et al., *Leading hadronic contribution to the muon magnetic moment from lattice QCD*, *Nature* **593** (2021), no. 7857 51–55, [[arXiv:2002.12347](#)].
- [13] C. Alexandrou et al., *Lattice calculation of the short and intermediate time-distance hadronic vacuum polarization contributions to the muon magnetic moment using twisted-mass fermions*, [arXiv:2206.15084](#).
- [14] M. Cè et al., *Window observable for the hadronic vacuum polarization contribution to the muon $g - 2$ from lattice QCD*, [arXiv:2206.06582](#).

- [15] G. Colangelo, A. X. El-Khadra, M. Hoferichter, A. Keshavarzi, C. Lehner, P. Stoffer, and T. Teubner, *Data-driven evaluations of Euclidean windows to scrutinize hadronic vacuum polarization*, [arXiv:2205.12963](#).
- [16] A. Crivellin, M. Hoferichter, C. A. Manzari, and M. Montull, *Hadronic Vacuum Polarization: $(g - 2)_\mu$ versus Global Electroweak Fits*, *Phys. Rev. Lett.* **125** (2020), no. 9 091801, [[arXiv:2003.04886](#)].
- [17] A. Keshavarzi, W. J. Marciano, M. Passera, and A. Sirlin, *Muon $g - 2$ and $\Delta\alpha$ connection*, *Phys. Rev. D* **102** (2020), no. 3 033002, [[arXiv:2006.12666](#)].
- [18] E. de Rafael, *Constraints between $\Delta\alpha_{\text{had}}(M_Z^2)$ and $(g_\mu - 2)_{\text{HVP}}$* , *Phys. Rev. D* **102** (2020), no. 5 056025, [[arXiv:2006.13880](#)].
- [19] B. Malaescu and M. Schott, *Impact of correlations between a_μ and α_{QED} on the EW fit*, *Eur. Phys. J. C* **81** (2021), no. 1 46, [[arXiv:2008.08107](#)].
- [20] G. Colangelo, M. Hoferichter, and P. Stoffer, *Constraints on the two-pion contribution to hadronic vacuum polarization*, *Phys. Lett. B* **814** (2021) 136073, [[arXiv:2010.07943](#)].
- [21] **CDF** Collaboration, T. Aaltonen et al., *High-precision measurement of the W boson mass with the CDF II detector*, *Science* **376** (2022), no. 6589 170–176.
- [22] M. Awramik, M. Czakon, A. Freitas, and G. Weiglein, *Precise prediction for the W boson mass in the standard model*, *Phys. Rev. D* **69** (2004) 053006, [[hep-ph/0311148](#)].
- [23] W. Altmannshofer, P. S. Bhupal Dev, and A. Soni, *$R_{D^{(*)}}$ anomaly: A possible hint for natural supersymmetry with R -parity violation*, *Phys. Rev.* **D96** (2017), no. 9 095010, [[arXiv:1704.06659](#)].
- [24] N. G. Deshpande and X.-G. He, *Consequences of R -parity violating interactions for anomalies in $\bar{B} \rightarrow D^{(*)}\tau\bar{\nu}$ and $b \rightarrow s\mu^+\mu^-$* , *Eur. Phys. J.* **C77** (2017), no. 2 134, [[arXiv:1608.04817](#)].
- [25] S. Trifinopoulos, *Revisiting R -parity violating interactions as an explanation of the B -physics anomalies*, *Eur. Phys. J.* **C78** (2018), no. 10 803, [[arXiv:1807.01638](#)].

- [26] W. Altmannshofer, P. B. Dev, A. Soni, and Y. Sui, *Addressing $R_{D^{(*)}}$, $R_{K^{(*)}}$, muon $g - 2$ and ANITA anomalies in a minimal R -parity violating supersymmetric framework*, *Phys. Rev. D* **102** (2020), no. 1 015031, [[arXiv:2002.12910](#)].
- [27] M.-D. Zheng and H.-H. Zhang, *Studying the $b \rightarrow s\ell^+\ell^-$ anomalies and $(g - 2)_\mu$ in R -parity violating MSSM framework with the inverse seesaw mechanism*, *Phys. Rev. D* **104** (2021), no. 11 115023, [[arXiv:2105.06954](#)].
- [28] Q.-Y. Hu, Y.-D. Yang, and M.-D. Zheng, *Revisiting the B -physics anomalies in R -parity violating MSSM*, *Eur. Phys. J. C* **80** (2020), no. 5 365, [[arXiv:2002.09875](#)].
- [29] P. S. Bhupal Dev, A. Soni, and F. Xu, *Hints of Natural Supersymmetry in Flavor Anomalies?*, [arXiv:2106.15647](#).
- [30] M.-D. Zheng, F.-Z. Chen, and H.-H. Zhang, *The $W\ell\nu$ -vertex corrections to W -boson mass in the R -parity violating MSSM*, [arXiv:2204.06541](#).
- [31] M. Blennow, P. Coloma, E. Fernández-Martínez, and M. González-López, *Right-handed neutrinos and the CDF II anomaly*, [arXiv:2204.04559](#).
- [32] F. Arias-Aragón, E. Fernández-Martínez, M. González-López, and L. Merlo, *Dynamical Minimal Flavour Violating Inverse Seesaw*, [arXiv:2204.04672](#).
- [33] J. Rosiek, *Complete Set of Feynman Rules for the Minimal Supersymmetric Extension of the Standard Model*, *Phys. Rev. D* **41** (1990) 3464.
- [34] J. Rosiek, *Complete set of Feynman rules for the MSSM: Erratum*, [hep-ph/9511250](#).
- [35] P. Bhupal Dev, S. Mondal, B. Mukhopadhyaya, and S. Roy, *Phenomenology of Light Sneutrino Dark Matter in c MSSM/ m SUGRA with Inverse Seesaw*, *JHEP* **09** (2012) 110, [[arXiv:1207.6542](#)].
- [36] A. K. Alok, A. Dighe, S. Gangal, and D. Kumar, *Continuing search for new physics in $b \rightarrow s\mu\mu$ decays: two operators at a time*, *JHEP* **06** (2019) 089, [[arXiv:1903.09617](#)].
- [37] J. Alda, J. Guasch, and S. Penaranda, *Anomalies in B mesons decays: a phenomenological approach*, *Eur. Phys. J. Plus* **137** (2022), no. 2 217, [[arXiv:2012.14799](#)].

- [38] A. Carvunis, F. Dettori, S. Gangal, D. Guadagnoli, and C. Normand, *On the effective lifetime of $B_s \rightarrow \mu\mu\gamma$* , *JHEP* **12** (2021) 078, [[arXiv:2102.13390](#)].
- [39] L.-S. Geng, B. Grinstein, S. Jäger, S.-Y. Li, J. Martin Camalich, and R.-X. Shi, *Implications of new evidence for lepton-universality violation in $b \rightarrow s\ell^+\ell^-$ decays*, *Phys. Rev. D* **104** (2021), no. 3 035029, [[arXiv:2103.12738](#)].
- [40] S.-Y. Li, R.-X. Shi, and L.-S. Geng, *Discriminating 1D new physics solutions in $b \rightarrow s\ell\ell$ decays*, *Chin. Phys. C* **46** (2022), no. 6 063108, [[arXiv:2105.06768](#)].
- [41] A. Angelescu, D. Bečirević, D. A. Faroughy, F. Jaffredo, and O. Sumensari, *Single leptoquark solutions to the B-physics anomalies*, *Phys. Rev. D* **104** (2021), no. 5 055017, [[arXiv:2103.12504](#)].
- [42] W. Altmannshofer and P. Stangl, *New physics in rare B decays after Moriond 2021*, *Eur. Phys. J. C* **81** (2021), no. 10 952, [[arXiv:2103.13370](#)].
- [43] C. Cornella, D. A. Faroughy, J. Fuentes-Martin, G. Isidori, and M. Neubert, *Reading the footprints of the B-meson flavor anomalies*, *JHEP* **08** (2021) 050, [[arXiv:2103.16558](#)].
- [44] J. Kriewald, C. Hati, J. Orloff, and A. M. Teixeira, *Leptoquarks facing flavour tests and $b \rightarrow s\ell\ell$ after Moriond 2021*, in *55th Rencontres de Moriond on Electroweak Interactions and Unified Theories*, 3, 2021. [arXiv:2104.00015](#).
- [45] G. Isidori, D. Lancierini, P. Owen, and N. Serra, *On the significance of new physics in $b \rightarrow s\ell^+\ell^-$ decays*, *Phys. Lett. B* **822** (2021) 136644, [[arXiv:2104.05631](#)].
- [46] M. Algueró, B. Capdevila, S. Descotes-Genon, J. Matias, and M. Novoa-Brunet, *$b \rightarrow s\ell^+\ell^-$ global fits after R_{K_S} and $R_{K^{*+}}$* , *Eur. Phys. J. C* **82** (2022), no. 4 326, [[arXiv:2104.08921](#)].
- [47] T. Hurth, F. Mahmoudi, D. M. Santos, and S. Neshatpour, *More Indications for Lepton Nonuniversality in $b \rightarrow s\ell^+\ell^-$* , *Phys. Lett. B* **824** (2022) 136838, [[arXiv:2104.10058](#)].
- [48] P. F. Perez, C. Murgui, and A. D. Plascencia, *Leptoquarks and matter unification: Flavor anomalies and the muon $g - 2$* , *Phys. Rev. D* **104** (2021), no. 3 035041, [[arXiv:2104.11229](#)].

- [49] J. Alda, J. Guasch, and S. Penaranda, *Anomalies in B mesons decays: Present status and future collider prospects*, in *International Workshop on Future Linear Colliders*, 5, 2021. [arXiv:2105.05095](#).
- [50] R. Bause, H. Gisbert, M. Golz, and G. Hiller, *Interplay of dineutrino modes with semileptonic rare B-decays*, *JHEP* **12** (2021) 061, [[arXiv:2109.01675](#)].
- [51] **LHCb** Collaboration, R. Aaij et al., *Angular analysis and differential branching fraction of the decay $B_s^0 \rightarrow \phi \mu^+ \mu^-$* , *JHEP* **09** (2015) 179, [[arXiv:1506.08777](#)].
- [52] G. Passarino and M. J. G. Veltman, *One Loop Corrections for $e^+ e^-$ Annihilation Into $\mu^+ \mu^-$ in the Weinberg Model*, *Nucl. Phys.* **B160** (1979) 151–207.
- [53] F. U. Bernlochner, M. F. Sevilla, D. J. Robinson, and G. Wormser, *Semitaquonic b-hadron decays: A lepton flavor universality laboratory*, *Rev. Mod. Phys.* **94** (2022), no. 1 015003, [[arXiv:2101.08326](#)].
- [54] D. Bryman, V. Cirigliano, A. Crivellin, and G. Inguglia, *Testing Lepton Flavor Universality with Pion, Kaon, Tau, and Beta Decays*, [arXiv:2111.05338](#).
- [55] P. Arnan, D. Becirevic, F. Mescia, and O. Sumensari, *Probing low energy scalar leptoquarks by the leptonic W and Z couplings*, *JHEP* **02** (2019) 109, [[arXiv:1901.06315](#)].
- [56] A. M. Coutinho, A. Crivellin, and C. A. Manzari, *Global Fit to Modified Neutrino Couplings and the Cabibbo-Angle Anomaly*, *Phys. Rev. Lett.* **125** (2020), no. 7 071802, [[arXiv:1912.08823](#)].
- [57] S. Antusch and O. Fischer, *Non-unitarity of the leptonic mixing matrix: Present bounds and future sensitivities*, *JHEP* **10** (2014) 094, [[arXiv:1407.6607](#)].
- [58] S. Antusch and O. Fischer, *Probing the nonunitarity of the leptonic mixing matrix at the CEPC*, *Int. J. Mod. Phys. A* **31** (2016), no. 33 1644006, [[arXiv:1604.00208](#)].
- [59] E. Fernandez-Martinez, J. Hernandez-Garcia, and J. Lopez-Pavon, *Global constraints on heavy neutrino mixing*, *JHEP* **08** (2016) 033, [[arXiv:1605.08774](#)].

- [60] **ATLAS** Collaboration, M. Aaboud et al., *Search for B - L R -parity-violating top squarks in $\sqrt{s} = 13$ TeV pp collisions with the ATLAS experiment*, *Phys. Rev. D* **97** (2018), no. 3 032003, [[arXiv:1710.05544](#)].
- [61] **CMS** Collaboration, A. M. Sirunyan et al., *Search for long-lived particles decaying into displaced jets in proton-proton collisions at $\sqrt{s} = 13$ TeV*, *Phys. Rev. D* **99** (2019), no. 3 032011, [[arXiv:1811.07991](#)].
- [62] **ATLAS** Collaboration, M. Aaboud et al., *Search for heavy charged long-lived particles in the ATLAS detector in 36.1 fb^{-1} of proton-proton collision data at $\sqrt{s} = 13$ TeV*, *Phys. Rev. D* **99** (2019), no. 9 092007, [[arXiv:1902.01636](#)].
- [63] **ATLAS** Collaboration, G. Aad et al., *Search for long-lived, massive particles in events with a displaced vertex and a muon with large impact parameter in pp collisions at $\sqrt{s} = 13$ TeV with the ATLAS detector*, *Phys. Rev. D* **102** (2020), no. 3 032006, [[arXiv:2003.11956](#)].
- [64] **ATLAS** Collaboration, G. Aad et al., *Search for R -parity-violating supersymmetry in a final state containing leptons and many jets with the ATLAS experiment using $\sqrt{s} = 13 \text{ TeV}$ proton-proton collision data*, *Eur. Phys. J. C* **81** (2021), no. 11 1023, [[arXiv:2106.09609](#)].
- [65] **CMS** Collaboration, A. M. Sirunyan et al., *Search for top squark production in fully-hadronic final states in proton-proton collisions at $\sqrt{s} = 13$ TeV*, *Phys. Rev. D* **104** (2021), no. 5 052001, [[arXiv:2103.01290](#)].
- [66] **CMS** Collaboration, A. Tumasyan et al., *Combined searches for the production of supersymmetric top quark partners in proton-proton collisions at $\sqrt{s} = 13$ TeV*, *Eur. Phys. J. C* **81** (2021), no. 11 970, [[arXiv:2107.10892](#)].
- [67] **ATLAS** Collaboration, M. Aaboud et al., *Search for supersymmetry in events with four or more leptons in $\sqrt{s} = 13$ TeV pp collisions with ATLAS*, *Phys. Rev. D* **98** (2018), no. 3 032009, [[arXiv:1804.03602](#)].
- [68] **ATLAS** Collaboration, M. Aaboud et al., *Search for lepton-flavor violation in different-flavor, high-mass final states in pp collisions at $\sqrt{s} = 13$ TeV with the ATLAS detector*, *Phys. Rev. D* **98** (2018), no. 9 092008, [[arXiv:1807.06573](#)].

- [69] **ATLAS** Collaboration, G. Aad et al., *Search for supersymmetry in events with four or more charged leptons in 139 fb^{-1} of $\sqrt{s} = 13\text{ TeV}$ pp collisions with the ATLAS detector*, *JHEP* **07** (2021) 167, [[arXiv:2103.11684](#)].
- [70] K. Agashe, M. Ekhterachian, Z. Liu, and R. Sundrum, *Sleptonic SUSY: From UV Framework to IR Phenomenology*, [arXiv:2203.01796](#).
- [71] **ATLAS** Collaboration, G. Aad et al., *Search for electroweak production of charginos and sleptons decaying into final states with two leptons and missing transverse momentum in $\sqrt{s} = 13\text{ TeV}$ pp collisions using the ATLAS detector*, *Eur. Phys. J. C* **80** (2020), no. 2 123, [[arXiv:1908.08215](#)].
- [72] **ATLAS** Collaboration, G. Aad et al., *Searches for electroweak production of supersymmetric particles with compressed mass spectra in $\sqrt{s} = 13\text{ TeV}$ pp collisions with the ATLAS detector*, *Phys. Rev. D* **101** (2020), no. 5 052005, [[arXiv:1911.12606](#)].
- [73] A. J. Buras, J. Girrbach-Noe, C. Niehoff, and D. M. Straub, *$B \rightarrow K^{(*)}\nu\bar{\nu}$ decays in the Standard Model and beyond*, *JHEP* **02** (2015) 184, [[arXiv:1409.4557](#)].
- [74] N. G. Deshpande and X.-G. He, *Consequences of R -parity violating interactions for anomalies in $\bar{B} \rightarrow D^{(*)}\tau\bar{\nu}$ and $b \rightarrow s\mu^+\mu^-$* , *Eur. Phys. J. C* **77** (2017), no. 2 134, [[arXiv:1608.04817](#)].
- [75] **Particle Data Group** Collaboration, P. A. Zyla et al., *Review of Particle Physics*, *PTEP* **2020** (2020), no. 8 083C01.
- [76] J. Aebischer, J. Kumar, P. Stangl, and D. M. Straub, *A Global Likelihood for Precision Constraints and Flavour Anomalies*, *Eur. Phys. J. C* **79** (2019), no. 6 509, [[arXiv:1810.07698](#)].
- [77] **Belle-II** Collaboration, F. Dattola, *Search for $B^+ \rightarrow K^+\nu\bar{\nu}$ decays with an inclusive tagging method at the Belle II experiment*, in *55th Rencontres de Moriond on Electroweak Interactions and Unified Theories*, 5, 2021. [arXiv:2105.05754](#).
- [78] **Belle** Collaboration, J. Grygier et al., *Search for $B \rightarrow h\nu\bar{\nu}$ decays with semileptonic tagging at Belle*, *Phys. Rev. D* **96** (2017), no. 9 091101, [[arXiv:1702.03224](#)].
[Addendum: *Phys.Rev.D* 97, 099902 (2018)].

- [79] T. Blake, G. Lanfranchi, and D. M. Straub, *Rare B Decays as Tests of the Standard Model*, *Prog. Part. Nucl. Phys.* **92** (2017) 50–91, [[arXiv:1606.00916](#)].
- [80] K. Earl and T. Grégoire, *Contributions to $b \rightarrow s\ell\ell$ Anomalies from R-Parity Violating Interactions*, *JHEP* **08** (2018) 201, [[arXiv:1806.01343](#)].
- [81] **LHCb** Collaboration, R. Aaij et al., *Search for the rare decay $D^0 \rightarrow \mu^+\mu^-$* , *Phys. Lett. B* **725** (2013) 15–24, [[arXiv:1305.5059](#)].
- [82] S. Nandi, S. K. Patra, and A. Soni, *Correlating new physics signals in $B \rightarrow D^{(*)}\tau\nu_\tau$ with $B \rightarrow \tau\nu_\tau$* , [arXiv:1605.07191](#).
- [83] Q.-Y. Hu, X.-Q. Li, Y. Muramatsu, and Y.-D. Yang, *R-parity violating solutions to the $R_{D^{(*)}}$ anomaly and their GUT-scale unifications*, *Phys. Rev.* **D99** (2019), no. 1 015008, [[arXiv:1808.01419](#)].
- [84] D. Buttazzo, A. Greljo, G. Isidori, and D. Marzocca, *B-physics anomalies: a guide to combined explanations*, *JHEP* **11** (2017) 044, [[arXiv:1706.07808](#)].
- [85] **LHCb** Collaboration, R. Aaij et al., *Precise determination of the $B_s^0\text{--}\overline{B}_s^0$ oscillation frequency*, *Nature Phys.* **18** (2022), no. 1 1–5, [[arXiv:2104.04421](#)].
- [86] **HFLAV** Collaboration, Y. Amhis et al., *Averages of b-hadron, c-hadron, and τ -lepton properties as of 2021*, [arXiv:2206.07501](#).
- [87] L. Di Luzio, M. Kirk, A. Lenz, and T. Rauh, *ΔM_s theory precision confronts flavour anomalies*, *JHEP* **12** (2019) 009, [[arXiv:1909.11087](#)].
- [88] B. de Carlos and P. L. White, *R-parity violation and quark flavor violation*, *Phys. Rev. D* **55** (1997) 4222–4239, [[hep-ph/9609443](#)].
- [89] **HFLAV** Collaboration, Y. S. Amhis et al., *Averages of b-hadron, c-hadron, and τ -lepton properties as of 2018*, *Eur. Phys. J. C* **81** (2021), no. 3 226, [[arXiv:1909.12524](#)].
- [90] M. Misiak et al., *Updated NNLO QCD predictions for the weak radiative B-meson decays*, *Phys. Rev. Lett.* **114** (2015), no. 22 221801, [[arXiv:1503.01789](#)].
- [91] I. Esteban, M. Gonzalez-Garcia, M. Maltoni, T. Schwetz, and A. Zhou, *The fate of hints: updated global analysis of three-flavor neutrino oscillations*, *JHEP* **09** (2020) 178, [[arXiv:2007.14792](#)].

- [92] J. S. Alvarado and R. Martinez, *PMNS matrix in a non-universal $U(1)_X$ extension to the MSSM with one massless neutrino*, [arXiv:2007.14519](#).
- [93] A. M. Abdullahi et al., *The Present and Future Status of Heavy Neutral Leptons*, in *2022 Snowmass Summer Study*, 3, 2022. [arXiv:2203.08039](#).
- [94] C. A. Argüelles et al., *Snowmass White Paper: Beyond the Standard Model effects on Neutrino Flavor*, in *2022 Snowmass Summer Study*, 3, 2022. [arXiv:2203.10811](#).
- [95] A. Abada, M. E. Krauss, W. Porod, F. Staub, A. Vicente, and C. Weiland, *Lepton flavor violation in low-scale seesaw models: SUSY and non-SUSY contributions*, *JHEP* **11** (2014) 048, [[arXiv:1408.0138](#)].
- [96] J. Chang, K. Cheung, H. Ishida, C.-T. Lu, M. Spinrath, and Y.-L. S. Tsai, *A supersymmetric electroweak scale seesaw model*, *JHEP* **10** (2017) 039, [[arXiv:1707.04374](#)].